

The Effect of Distant Encounters on Black Hole Binaries in Globular Clusters: Systematic Increase of In-cluster Mergers in the LISA band

Johan Samsing¹, Adrian S. Hamers², Jacob G. Tyles¹

¹*Department of Astrophysical Sciences, Princeton University,
Peyton Hall, 4 Ivy Lane, Princeton, NJ 08544, USA.*

²*Institute for Advanced Study, School of Natural Sciences, Einstein Drive, Princeton, NJ 08540, USA.*

We present the first systematic study on how distant weak interactions impact the dynamical evolution of merging binary black holes (BBHs) in dense stellar clusters. Recent studies indicate that dense clusters are likely to significantly contribute to the rate of merging BBHs observable through gravitational waves (GWs), and that many of these mergers will appear with notable eccentricities measurable in the LISA and LIGO sensitivity bands. This is highly interesting, as eccentricity can be used to distinguish between different astrophysical merger channels. However, all of these recent studies are based on various Monte Carlo (MC) techniques that only include strong interactions for the dynamical evolution of BBHs, whereas any binary generally undergoes orders-of-magnitude more weak interactions than strong. It is well known that weak interactions primarily lead to a change in the binary’s eccentricity, which for BBHs implies that weak interactions can change their GW inspiral time and thereby their merger probability. With this motivation, we perform MC simulations of BBHs evolving in dense clusters under the influence of both weak and strong interactions. We find that including weak interactions leads to a notable increase in the number of BBHs that merge inside their cluster, which correspondingly leads to a higher number of eccentric LISA sources. These preliminary results illustrate the importance of including weak interactions for accurately modeling how BBHs merge in clusters, and how to link their emitted GW signals to their astrophysical environment.

I. INTRODUCTION

The origin of binary black hole (BBH) mergers is still unknown, despite several now have been directly observed through their emission of gravitational waves (GWs) [1–7]. The currently observed set shows great variety in both the BH mass spectrum, and BH spins [e.g. 8]. At least one neutron star (NS) merger has also been observed [9] in addition to several peculiar low signal-to-noise events, and this variety therefore indicates that several formation channels might be at play. Some of the recently proposed channels include: field binaries [10–18], dense stellar clusters [19–27], active galactic nuclei (AGN) discs [28–30], galactic nuclei (GN) [31–37], very massive stellar mergers [38–41], and single-single GW captures of primordial black holes [42–45].

The key exercise is how to observationally tell these channels apart; several observables have been suggested. For example, an electromagnetic (EM) signal might be associated with both BBH mergers in AGN discs and those coming from rapidly rotating stars, in contrast to gas-free isolated BBH mergers found in, e.g., stellar clusters and the field. Tidal disruption events (TDE) associated with stars disrupted by BBHs in dense stellar clusters might also be used to probe the merger history of BBHs [46–48]. Other ways of ‘lightning up’ single or binary BHs through TDEs include, e.g., BHs kicked into disruptive orbits from either dynamics, GW recoils or direct collapse following supernova [e.g. 49, 50]. Such multi-messenger (EM+GW) observables are interesting, but unfortunately also highly uncertain to both accurately predict and model. More promising are proper-

ties that can be read off directly from the incoming GW waveform, which include the BBH masses and spins, the orbital eccentricity, and even doppler effects related to a possible movement of the BBH’s center of mass (COM) [e.g. 51, 52]. For example, the spins are expected to be isotropically distributed for BBH mergers forming in clusters, in contrast to field BBH mergers [e.g. 53, 54]. BBHs assembled in clusters through chaotic few-body interactions have also recently been shown to lead to a non-negligible unique population of mergers with measurable eccentricities in all bands from LISA (the Laser Interferometer Space Antenna) [55–57] to LIGO (the Laser Interferometer Gravitational Wave Observatory) [58–67]. Eccentric sources can form in other ways, e.g. through Lidov-Kozai oscillations [e.g. 68–74], quadruple systems [e.g. 75], and single-single GW captures [e.g. 31, 43, 76, 77], but eccentric cluster mergers are unavoidably produced if BHs are present in clusters, in particular globular clusters (GCs), and therefore constitute a highly useful diagnostic for the cluster channel.

The topic of this paper is on how BBHs are dynamically driven to merger in GCs under the influence of both weak and strong interactions, as well as what unique GW signals to expect from this population. BBHs in GCs generally form through single-single-single interactions [e.g. 78–80] in the cluster center, where the mass segregated BH population constitute a highly dense BH subsystem [e.g. 81, 82]. Each BBH formed in this way is initially very wide and will not merge within a Hubble time, but subsequent interactions with incoming single BHs lead to shrinkage of the orbit, referred to as hardening, and large changes in the eccentricity [e.g. 78]. This eventually drives the BBH to merger either in-side or out-side of

its cluster. Current state-of-the-art Monte Carlo (MC) cluster codes aimed at modeling the evolution of such BBHs, including the CMC code [67] and the MOCCA code [83], incorporate only the effects from strong encounters, and include therefore not the potential importance of the many more weak encounters a given BBH undergoes during its life inside its cluster.

In this work we present the first study on how the numerous number of unbound weak encounters a BBH undergoes in-between each strong encounter affects its dynamical evolution and GW merger properties. Each of these weak encounters changes the eccentricity of the BBH, which leads to a non-linear and asymmetric random walk with varying step sizes, also known as a quasi-Levy flight, in-between each strong encounter. In classical cluster dynamics where post-Newtonian (PN) corrections [e.g. 84] are not included and all objects are assumed to be point-like, weak encounters are not important as the associated energy exchange is exponentially suppressed; however, when dissipative effects, such as PN corrections, tides, and finite sizes are included, objects from ordinary stars to BHs can be driven to merger through high eccentricity orbits [e.g. 85]. Such eccentricity driven mergers not only give rise to interesting observables, including GWs, TDEs, and jetted EM sources, but will also change the energy balance of the cluster and thereby its large scale dynamics.

We here explore the combined effects from strong and weak three-body encounters using analytical and numerical methods, and investigate how their interplay drives BBHs to merger in dense clusters. For this we particularly make use of the strong scattering model presented in [64] and [55], and our new second-order weak interaction solution presented in [86], referred to as HS19, which expands upon the first-order solution presented in [87], referred to as HR96. We find that the inclusion of weak interactions leads to notable changes in both the number of BBHs merging inside their cluster and their distribution across GW peak frequency and orbital eccentricity. This leads us to conclude that weak encounters are important to include for an accurate modeling of how BBHs merge in clusters, which is naturally an increasingly relevant inquiry now that there is a growing population of observed GW events. This poses some interesting challenges, as the leading numerical schemes which include the Hénon method in the field of PN dynamics do not easily allow for the inclusion of weak encounters. We also highlight the importance of using the second-order results from HS19, which solve some crucial problems occurring when using the expressions of HR96 for evolving BBHs in the high eccentricity regime.

The paper is organized as follows. We start by describing the outcome of a single weak encounter in Section II. This includes a discussion of why distant encounters must be important for an accurate modeling of BBH mergers, and several new dynamical effects that have not yet been properly described in the literature related to this subject. After this, we study in Section III a population of

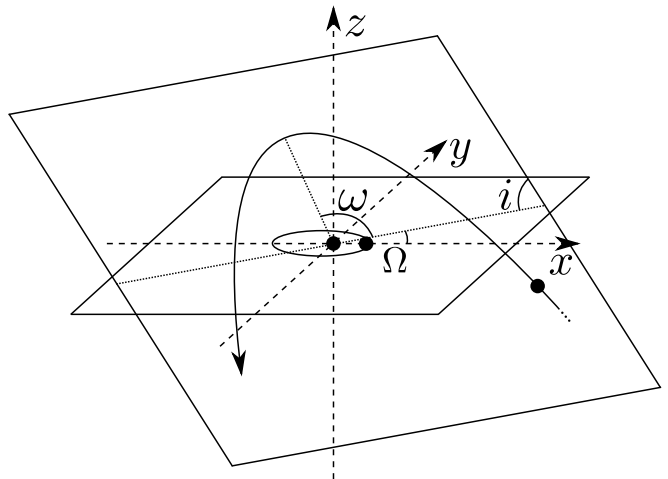


FIG. 1. Illustration showing how we define our orbital elements used throughout the paper. The binary is positioned in the x, y -plane with its peri-center pointing along the x -axis, where the perturber is here illustrated to encounter the binary in its own unperturbed plane on a counter-clockwise orbit. The black dots denoting the three interacting objects, and the solid lines showing their orbits, are not to scale and just added for illustrative purposes. We use ‘standard angles’ defined as follows: Ω is the longitude of the ascending node measured in the plane of motion of the binary, i is the inclination between the two orbital planes, and ω is the longitude of peri-center of the third body measured in its plane of motion from the ascending node. Our definitions are identical to the one used in HR96, where further details can be found.

BBHs and how they evolve under the influence of both strong and weak encounters. For this we use numerical and analytical techniques combined with MC methods. We discuss and conclude our findings in Section IV.

II. A SINGLE WEAK ENCOUNTER

We start by exploring the range of outcomes associated with a single weak encounter between a BBH and a single incoming BH. For this, we consider a BBH with initial orbital eccentricity e_0 and semi-major axis (SMA) a_0 interacting with an incoming BH on a parabolic orbit. Here, and in the rest of the paper, we assume the interacting BHs all have the same mass m . For describing the ICs we make use of the standard orbital angles shown in Figure 1, which is further described in HR96. Note here that these are different from the set used in HS19 (see Section 2.1 in the latter paper).

A. Background and Motivation

For binary-single interactions to be in the secular regime, the mean motion of the binary must be much greater than the orbital speed of the single at the time

of peri-center passage (HR96). In this limit, the binary-single equations-of-motion (EOM) can be written out using a technique known as ‘orbital averaging’, which is widely used for e.g. studying the hierarchical bound-triple Lidov-Kozai problem [e.g. 88]. In the case where the third object is on an unbound orbit with an initial eccentricity E , the orbital averaged EOM naturally gives rise to the following parameter ϵ , which appears as a common factor in the EOM (HS19),

$$\epsilon = \left[\frac{M^2}{m_b(m_b + M)} \left(\frac{a_0}{r_p} \right)^3 (1 + E)^{-3} \right]^{1/2}, \quad (1)$$

where m_b is the mass of the BBH ($m_b = 2m$), M is the mass of the perturber ($M = m$), and r_p is the distance between the BBH center-of-mass (COM) and the incoming BH at the time of peri-center passage. As seen, weak interactions for which $r_p/a_0 \gg 1$ are characterized by having $\epsilon \ll 1$.

The main effect from a BBH undergoing a weak interaction with a single incoming BH is a change in the orbital eccentricity of the BBH, Δe , such that the final eccentricity after the encounter is $e_{\text{fin}} = e_0 + \Delta e$. The change Δe can to first-order (FO) in ϵ in the parabolic limit be analytically expressed as (HR96),

$$\Delta e_{\text{FO}} = -\epsilon \frac{15\pi}{4} e_0 \sqrt{1 - e_0^2} \sin 2\Omega \sin^2 i, \quad (2)$$

where Ω is the longitude of the ascending node measured in the plane of motion of the binary, and i is the inclination between the two orbital planes of the binary and the perturber, respectively, as further described in Fig. 1. Note here that this term has been derived by expanding the EOM to lowest non-trivial order in the (assumed to be) small ratio of the binary separation to the distance between the binary COM and the perturber, i.e., it is only accurate to quadrupole order. As shown in HR96, this expression accurately fits numerical simulations for $r_p/a_0 \gg 1$ and intermediate values of e_0 , and have therefore been widely used as a replacement for otherwise computationally demanding three-body simulations [e.g. 89]. HR96 also presented solutions to the $e_0 = 0$ limit, and in regions where the secular approach breaks down. However, one consideration not addressed in HR96 is the regime where $\Delta e \approx 1 - e_0$, which is possible if e_0 is near unity. For describing the formation of BBH mergers in dense clusters this is a highly relevant limit, as basically all mergers form through high eccentricity orbits. It is known that BBHs can be driven to very high eccentricities entirely through strong few-body encounters, i.e. without any assistance from weak interactions (see e.g. [64]); however, binaries undergoing strong interactions will also undergo numerous weak interactions in-between each strong interaction each of which will perturb the binary [e.g. 89]. The question is if a model that also includes weak interactions will lead to more or less mergers from high eccentricity orbits.

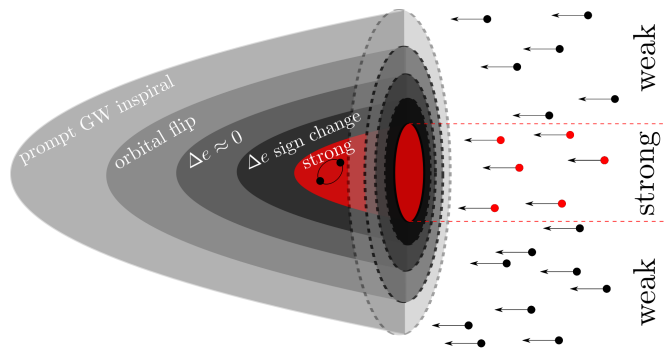


FIG. 2. Illustration of a binary interacting with an incoming population of single objects, where the strong interaction regime is highlighted in red, and the weak interaction regime in grey. The weak regime is further divided into different sub-regimes, each giving rise to a distinct type of outcome. The range of outcome types depends on the ICs, the shown here are the ones relevant for our fiducial parameters outlined in the end of Section II A. As described in Section II, the outcomes of a binary-single interaction with our chosen ICs can, from high to low values of r_p/a_0 , broadly be divided into the following regimes: (i) Distant weak interaction regime. Here the change in binary eccentricity is relatively small, and can be described using FO theory. For our ICs $\Delta e > 0$. (ii) Prompt GW inspiral regime. Here the final eccentricity is $e_{\text{fin}} \approx 0$, which results in a prompt GW inspiral merger during the interaction. This also marks the limit below which SO theory has to be used. (iii) Orbital flip regime. Below this limit the orbital angular momentum vector flips around during the interaction. (iv) $\Delta e \approx 0$ regime. The final eccentricity is here $e_{\text{fin}} \approx e_0$, implying $\Delta e \approx 0$. (v) Δe sign-change regime. After crossing $e_{\text{fin}} = e_0$ from above the binary here ends up with $e_{\text{fin}} < e_0$, i.e. $\Delta e < 0$. (vi) Strong regime. The binary here undergoes a strong interaction with an outcome that can be described using probability theory. In Section III we consider the evolution of a BBH undergoing strong and weak interactions inside a dense cluster.

To gain insight into this and motivate our present study, we now consider the following simple cluster model: we consider a cluster core described by a BH subsystem with a constant density and velocity dispersion, and assume that all BH interactions take place in this system and only involve objects of similar mass. This model provides in fact a good description of real cluster cores, as BHs both are expected to segregate, separate in mass, and clear out the center, as a result of mass segregation. In this picture, if only strong binary-single encounters are included in the cluster dynamics, a BBH will merge in-between its interactions if its GW inspiral life time [90],

$$\tau \approx \frac{768}{425} \frac{5c^5}{512G^3} \frac{a^4}{m^3} (1 - e^2)^{7/2}, \quad (3)$$

is less than its strong encounter (SE) time, t_{SE} , defined as the time it takes for the BBH to undergo its next strong

interaction [e.g. 55],

$$t_{\text{SE}} \approx \frac{1}{12\pi G} \frac{v_{\text{dis}}}{n_s m a}, \quad (4)$$

where n_s is the number density of single BHs in the cluster, v_{dis} is the cluster velocity dispersion, a is the SMA of the BBH, and e is its eccentricity. This correspondingly implies that a BBH with an eccentricity $e > e_{\text{SE}}$,

$$e_{\text{SE}} \approx \sqrt{1 - (t_{\text{SE}}/\tau_c)^{2/7}}, \quad (5)$$

where τ_c denotes the time for which $e = 0$ in Eq. (3), will undergo a merger before its next strong binary-single interaction. For a BBH with $a = 1 \text{ AU}$, $m = 20 M_\odot$, $n_s = 10^5 \text{ pc}^{-3}$, and $v_{\text{dis}} = 10 \text{ kms}^{-1}$, one finds $e_{\text{SE}} \approx 0.99$. This is a relatively high eccentricity, which means that even small changes of order $\Delta e \sim 1 - 0.99 \sim 10^{-2}$ can change the state and outcome of the BBH, from e.g. surviving to merging. Now, changes of such magnitude can easily be provided by weak interactions; the question is then, will weak interactions on average prevent or help a BBH to merge if its eccentricity is already near the critical value e_{SE} ? As pointed out above, the FO result Δe_{FO} presented in HR96 breaks down in this high eccentricity limit, and will therefore often lead to unphysical results such that $e_{\text{fin}} \geq 1$.

To resolve this problem with the FO solution in the high eccentricity limit, we used in our companion paper HS19 second-order (SO) perturbation theory to derive higher order correction terms to Δe . In short, in the FO approximation of HR96, the binary orbital components are assumed to be fixed while integrating over the passage of the perturber (this is analogous to ‘double averaging’ in hierarchical triple systems). Instead, in HS19 we used Fourier expansions to take into account the instantaneous response of the binary to the perturber while integrating over the latter’s passage. This resulted in an expression for the eccentricity change to SO in ϵ , which in the limit of small eccentricity changes and parabolic perturbers reads,

$$\begin{aligned} \Delta e_{\text{SO}} = \Delta e_{\text{FO}} + \epsilon^2 \frac{3}{512} \pi e_0 \left[-100 (1 - e_0^2) \sin 2\Omega \right. & (6) \\ \left. \left\{ (5 \cos i + 3 \cos 3i) \cos 2\omega + 6 \sin i \sin 2i \right\} \right. \\ + 4 \cos 2i \left\{ 3\pi (81e_0^2 - 56) - 200 (1 - e_0^2) \right. & \\ \left. \left. \cos 2\Omega \sin 2\omega \right\} + 3\pi \left\{ 200e_0^2 \sin^4 i \cos 4\Omega \right. \right. & \\ + 8 (16e_0^2 + 9) \sin^2 2i \cos 2\Omega & \\ \left. \left. + (39e_0^2 + 36) \cos 4i - 299e_0^2 + 124 \right\} \right], & \end{aligned}$$

where the introduced set of angles $\{i, \Omega, \omega\}$ are shown and defined in Fig. 1. We reiterate that the orbital an-

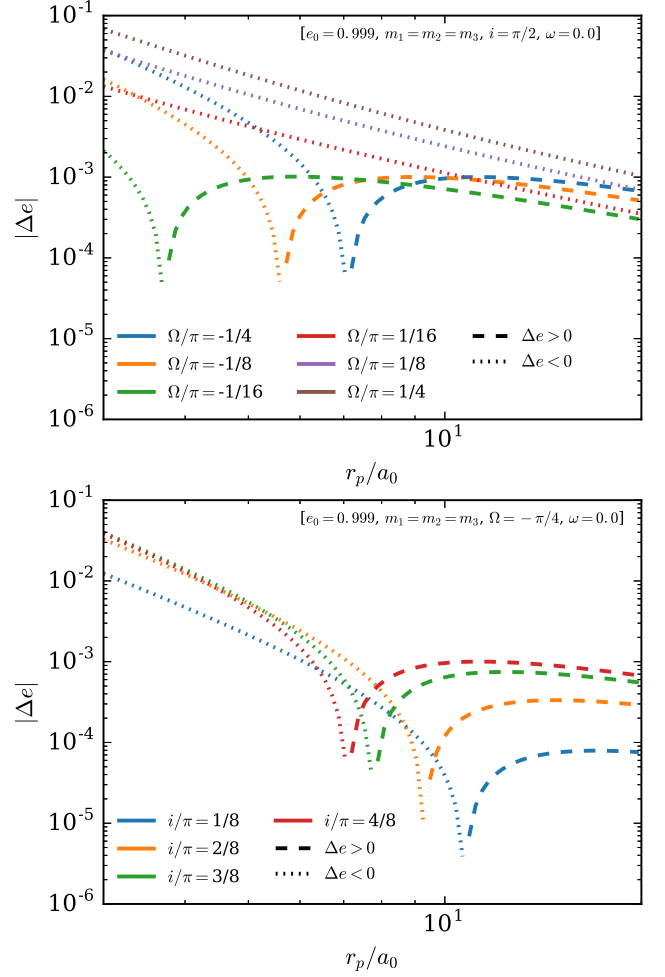


FIG. 3. Change in eccentricity, Δe , derived using our SO solution given by Eq. (6). The FO solution given by Eq. (2), always predicts a simple power-law change of the form $\Delta e \propto (r_p/a_0)^{-3/2}$. The large variations seen above are therefore due to corrections from the SO term $\propto \epsilon^2$. In the above plots, the *dashed* and *dotted* lines show the change in eccentricity for $\Delta e > 0$ and $\Delta e < 0$, respectively, where the different *colored* lines show results for different values of the orbital angles, as specified in the legends. The initial values that are kept fixed are shown in the upper right corner in each plot. As seen, in the *top plot* the inclination $i = \pi/2$ and Ω is varied, where in the *bottom plot* the angle $\Omega = -\pi/4$ and the inclination i is varied. The SO term gives rise to very important and easily notable corrections that greatly differ from the FO prediction, which includes sign changes, orbital spin flips, and a different power-law scaling for very close encounters. This is further described in Section II. A comparison to full numerical scatterings is shown in Fig. 4 and HS19. Finally, one should note that when 1,2PN are included any reference to initial orbital elements is ill-defined due to precession. For this reason, we do not include lower PN terms for this and similar figures, which are aimed at giving a clear overview of outcomes. In reality, precession will to ‘first order’ just add to a randomization of the initial orbital elements, which is naturally taken into account in standard MC experiments.

gles used here are defined differently than in HS19. As for Δe_{FO} , this term is only accurate to quadrupole order. The second term that is SO in ϵ , resolves many problems associated with only using the FO term Δe_{FO} , as further explained in HS19. Note here that all dependencies on mass and closest approach only enter via the ϵ term. A few examples of Δe_{SO} , as a function of the peri-center distance of the perturber w.r.t to the COM of the BBH scaled by the initial SMA, r_p/a_0 , are shown and discussed in Fig. 3. As seen, the SO correction clearly breaks the simple FO power-law solution. This will be described in greater detail later. Finally, one should note that the SO solution is still only accurate to quadrupole order and will therefore break down when r_p/a_0 starts to approach unity, and/or when the binary's component masses are unequal. In contrast, the FO solution can break down at *any* r_p/a_0 , i.e. also in highly secular regions, depending on the initial eccentricity. The improvements from including octupole terms (the next non-trivial-order terms in the expansion of the small ratio of the binary separation to the distance between the binary COM and the perturber), as well as higher-order terms in ϵ (i.e., third order), will be explored in upcoming work.

In the subsections below we systematically describe the outcomes of a BBH undergoing a single weak encounter, and the associated novel features that are not captured by the classical FO result Δe_{FO} from HR96. All our results are based on the initial set of orbital angles $i = \pi/2$, $\Omega = -\pi/4$, $\omega = 0$, a set we loosely refer to as our ‘fiducial parameters’, to match previous results from HR96 for easy comparison. We therefore here focus on the dependence on r_p/a , but we will in an upcoming paper present further discussions on the dependence on the initial set of orbital angles. An illustration outlining the different outcomes associated with our choice of fiducial parameters is shown in Fig. 2.

B. Distant weak encounters

We start by considering the top plot in Fig. 4, which shows $|\Delta e| = |e_{\text{fin}} - e_0|$ as a function of r_p/a_0 . The dashed-dotted lines show the FO result Δe_{FO} from HR96 (Eq. (2)), the dotted lines show the SO result Δe_{SO} from HS19 (Eq. (6)), where the symbols show results from a full three-body integration using the N -body code used in [65, 85, 91]. Note here that only one simulation is performed per point, which naturally gives rise to Poisson scatter.

The numerical and the analytical results clearly approach the simple power-law solution $\Delta e \propto (r_p/a_0)^{-3/2}$ given by Eq. (2) in the asymptotic limit $r_p \gg a$. The slope value $-3/2$ is universal in the sense that it does not depend on the mass ratio or the angular configurations of the three-body system. This universality provides some insight into the role of how important a constant flux of distant encounters might be for the eccentricity evolution. Especially, we might ask the question: does a uni-

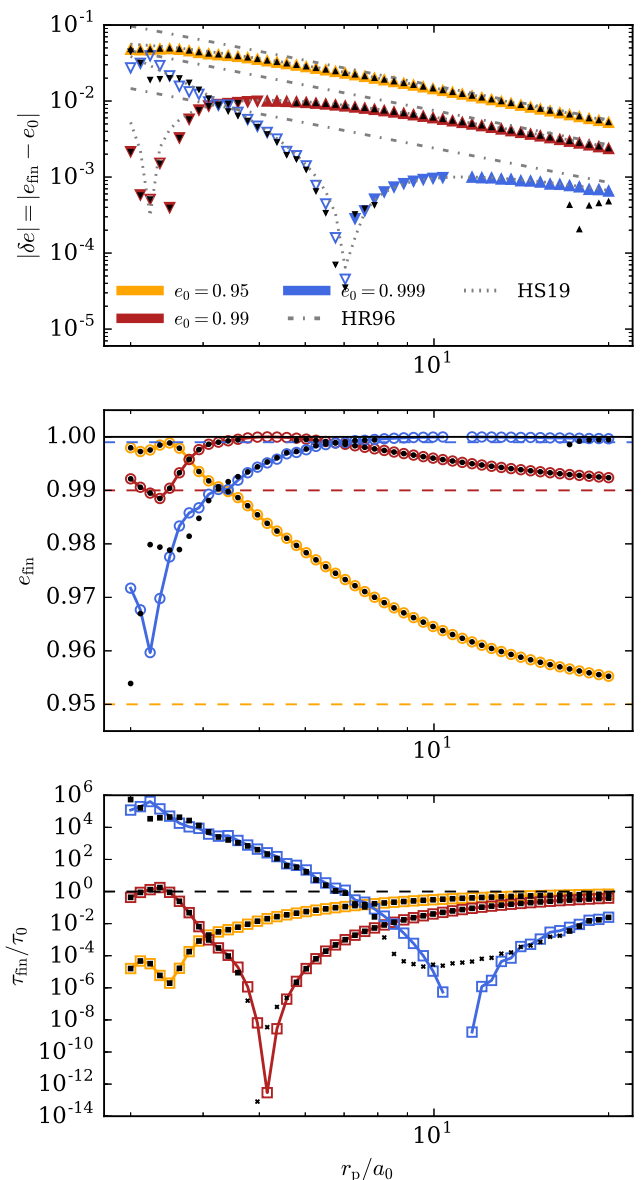


FIG. 4. Results from weak binary-single interactions between three equal mass BHs for varying values of e_0 (orange/red/blue) and r_p/a_0 (x-axis). For all scatterings we assume: $i = \pi/2$, $\Omega = -\pi/4$, $\omega = 0$, $m = 20M_\odot$, and $a_0 = 0.5$ AU. The *plot symbols* denote results from full numerical three-body integrations, where the larger *colored symbols* show results from including Newtonian forces only, and the smaller *black symbols* show results from additionally including the 2.5PN term. *Top plot*: Change in eccentricity $|\Delta e|$. The *full* and *empty* symbols denote $\Delta e > 0$ and $\Delta e < 0$, respectively, where an upwards (downwards) pointing *triangle symbol* denotes $\text{sign}(J_{\text{BH}z}) = +1(-1)$. The *grey dashed-dotted lines* show predictions from the FO solution given by Eq. (2) (HR96), where the *grey dotted lines* show predictions from our SO result given by (6) (HS19). *Middle plot*: Final eccentricity e_{fin} . The *dashed lines* are here showing the initial values e_0 . *Bottom plot*: GW inspiral time of the binary after the interaction, τ_{fin} , scaled by the initial value τ_0 . The *black crosses* denote outcomes for which the BBH merges during the weak interaction.

form and infinite sea of weak encounters lead to a divergent result? To gain some insight into this we first notice that the number of single encounters dN_s per time interval dt , Γ_s , with $r_p < R_p$ under the assumption of constant number density and velocity dispersion is $\propto R_p$ [62]. This implies that the rate per peri-center interval $d\Gamma_s/dr_p \propto k$, where k is a constant. Let us now consider a ‘worst case scenario’ where all single encounters lead to the same positive change in eccentricity $\Delta e_+ \propto (r_p/a_0)^{-3/2}$ (note that $\langle \Delta e \rangle = 0$ to FO, but not the variance). Assuming all the eccentricity changes are uncorrelated, one finds in this case that the total change in eccentricity, $d\Delta e_{\text{tot}}$, per unit time, dt , from single encounters in the range $r_{p,\text{min}}$ to $r_{p,\text{max}}$ is given by

$$\frac{d\Delta e_{\text{tot}}}{dt} \propto \int_{r_{p,\text{min}}}^{r_{p,\text{max}}} \frac{d\Gamma_s}{dr_p} \Delta e_+ dr_p \propto \frac{1}{\sqrt{r_{p,\text{min}}}} - \frac{1}{\sqrt{r_{p,\text{max}}}}. \quad (7)$$

This term does not diverge when setting the upper limit $r_{p,\text{max}} = \infty$, which illustrates that the rate of eccentricity change from even an infinite number of distant encounters all leading to a positive change $\Delta e_+ \propto (r_p/a_0)^{-3/2}$, does not lead to a diverging result. We therefore expect our results to converge as the upper value of r_p in our analysis increases; a value we generally will refer to as R_p . We note here that an accurate analytical modeling of how the eccentricity changes over time from close and distant encounters can be done using a Boltzmann-approach, which requires the derivation of diffusion coefficients. We will do that in an upcoming paper. In this paper we will be using numerical MC techniques, as described later in Section III.

Finally, the discussions from this section are based on a Newtonian treatment of the problem; however, when PN terms are included several changes are expected from especially precession, which will make the ICs ill-defined and also modify the simple asymptotic solution $\Delta e \propto (r_p/a_0)^{-3/2}$. This will be discussed further in Section II E.

C. Orbital flip and prompt GW Inspiral

We now consider lower values of r_p/a_0 where the FO power law solution $\Delta e \propto (r_p/a_0)^{-3/2}$ from Eq. (2) starts to break down. Considering our examples, we see in the top plot of Fig. 4 that for BBHs with an initial eccentricity $e_0 = 0.95$, $e_0 = 0.99$, and $e_0 = 0.999$ that the FO estimates start to deviate from the numerically estimated (correct) solutions for $r_p/a_0 \lesssim 5$, $r_p/a_0 \lesssim 7$, and $r_p/a_0 \lesssim 20$, respectively. Generally, the value for r_p/a_0 below which the FO result starts to break down, a value we denote $(r_p/a_0)_{\text{FO}}^{\text{BR}}$, is where the change in eccentricity Δe is comparable to $1 - e_0$, i.e. where the final eccentricity $e_{\text{fin}} \approx 1$. The physical boundary $e = 1$ for bound orbits is not built into the the FO solution, therefore the decrease seen in the figure for the numerically estimated value of Δe compared to the FO power law prediction

for $(r_p/a_0) \lesssim (r_p/a_0)_{\text{FO}}^{\text{BR}}$ originates to simply ‘prevent’ the BBH for reaching values of $e_{\text{fin}} > 1$. This statement is further supported by considering the middle plot of Fig. 4, which shows e_{fin} as a function of r_p/a_0 .

An approximate value for $(r_p/a_0)_{\text{FO}}^{\text{BR}}$ can be found by considering the relation $\Delta e = 1 - e_0 = \Delta e_{\text{FO}}$ and then solve for r_p/a_0 . In the parabolic equal mass limit one finds,

$$(r_p/a_0)_{\text{FO}}^{\text{BR}} \approx \left[\frac{e_0 \sqrt{1 - e_0^2}}{e_0 - 1} \frac{15\pi \sin 2\Omega \sin^2 i}{16\sqrt{3}} \right]^{2/3}. \quad (8)$$

For our ‘fiducial orbital parameters’ listed in Section II A and for $e_0 = 0.99$, one finds using the above relation $(r_p/a_0)_{\text{FO}}^{\text{BR}} \approx 8$, which indeed provides a reasonable estimate for when FO theory starts to break down. In the limit of very high initial eccentricity one finds that $(r_p/a_0)_{\text{FO}}^{\text{BR}} \propto (1 - e_0)^{-1/3}$, which shows that for $e_0 = 1 - 10^{-x}$ the break value $(r_p/a_0)_{\text{FO}}^{\text{BR}} \propto 10^{x/3}$. One decade closer to $e = 1$ therefore moves the break value up by about a factor of 2. Finally, one should note that for decreasing values of e_0 the value of $(r_p/a_0)_{\text{FO}}^{\text{BR}}$ correspondingly approaches 1 in which case the secular formalism breaks down. The above relation is therefore only useful for BBHs with an initial high eccentricity.

We now focus on our SO expression Δe_{SO} given by Eq. (6), which is shown with dotted lines in the top plot of Fig. 4. As seen here and further discussed in HS19, this relation accurately captures the correct physical form for Δe and thereby resolves the problems associated with the FO result near and below $(r_p/a_0)_{\text{FO}}^{\text{BR}}$. The decrease in Δe given by the SO relation that ensures that $e_{\text{fin}} < 1$ originates from the second term $\propto \epsilon^2$ in Eq. (6), which in this case has a sign opposite to the FO term $\propto \epsilon$. As shown in HS19, the location of r_p/a_0 for which Δe is maximized, i.e. the location of the plateau seen in the plot of Δe slightly below $(r_p/a_0)_{\text{FO}}^{\text{BR}}$, can be analytically calculated. As in HS19, we refer to the (r_p/a_0) location of the plateau by $(r_p/a_0)_{\text{plateau}}$. The solution for $(r_p/a_0)_{\text{plateau}}$ follows from solving the equation $\partial \Delta e_{\text{SO}} / \partial (r_p/a_0) = 0$, where Δe_{SO} is given by Eq. (6). The solution is long, but can easily be written out in closed form, which provides a clear expression for when SO terms are important (See HS19 for further details).

The dynamics near the plateau are highly interesting, and we now explore them in greater detail. First, we find that as one passes the plateau from high to low values of r_p/a_0 , the component of the BBH orbital angular momentum vector projected along the initial ‘z-axis’ (perpendicular to the orbital plane of the BBH), denoted here by $J_{\text{BH}z}$, changes sign; a behavior we denote *orbital flipping*. Loosely speaking, the vector component $J_{\text{BH}z}$ flips around, from $\text{sign}(J_{\text{BH}z}) = +1$ to $\text{sign}(J_{\text{BH}z}) = -1$, as the BBH ‘reflects off’ the $e = 1$ boundary near $(r_p/a_0)_{\text{plateau}}$. The final BBH therefore spins in the opposite direction compared to its orbital spin vector prior to the interaction. The sign change is also shown in

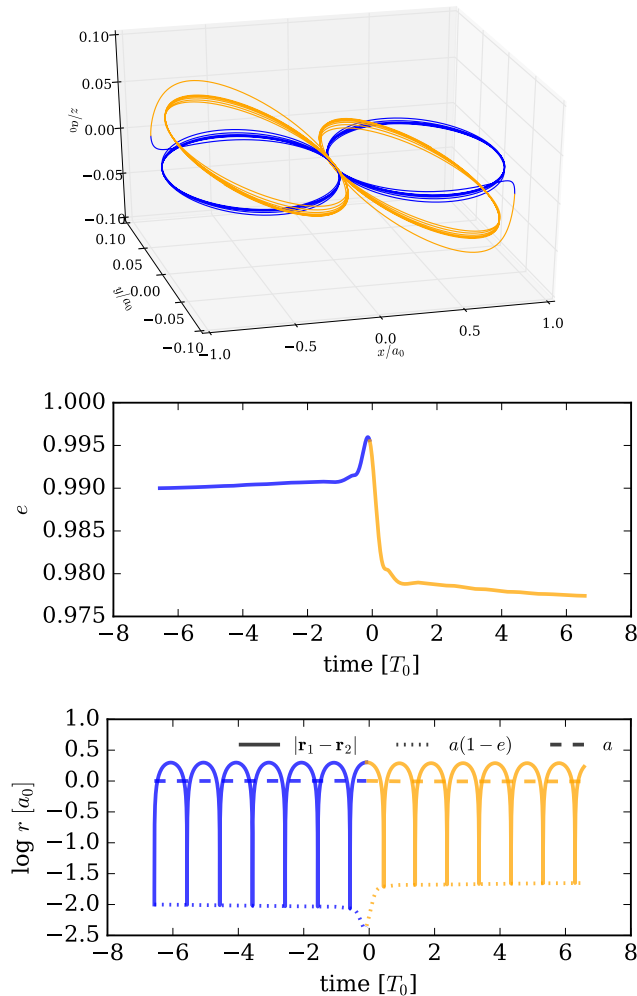


FIG. 5. Binary evolution during a single weak encounter with initial orbital parameters: $r_p/a_0 = 3.0$, $e_0 = 0.99$, and $i = \pi/2$, $\Omega = -\pi/4$, $\omega = 0$. The *line colors* denote the sign of the BBH orbital angular momentum vector along the z -axis, where blue (orange) shows the part of the orbit where $\text{sign}(J_{\text{BH}z}) = +1$ ($\text{sign}(J_{\text{BH}z}) = -1$). The initial $J_{\text{BH}z}$ is aligned with the z -axis, and the change from blue to orange therefore illustrates how the orbit ‘flips around’. The simulations do not include PN effects. *Top plot*: Illustration of the actual BBH orbits printed out from our three-body integrator. As seen, the encounter in this example courses the BBH orbit to flip on a time scale shorter than the BBH orbital time. *Middle plot*: Corresponding evolution of the BBH orbital eccentricity calculated from its osculating elements. In FO theory Δe would be so large that $e_{\text{fin}} > 1$ (see e.g. Fig. 4). However, this is not what physically happens. Instead, the BBH first approaches $e \sim 1$ after which it flips around and continue its evolution on a counter rotating orbit. *Bottom plot*: Distance, $|\mathbf{r}_1 - \mathbf{r}_2|$, osculating peri-center distance, $a(1-e)$, and SMA, a , of the BBH as a function of time. From the osculating peri-center distance one would naively conclude that the two BHs undergo a very close passage and possible merger during the orbital flip; however, as the flip happens almost instantaneously, the two BHs never get particularly close as seen when comparing to $|\mathbf{r}_1 - \mathbf{r}_2|$. These results are further discussed in Section II C and II D.

the upper plot of Fig. 4, where the triangles pointing upwards indicate no sign change ($\text{sign}(J_{\text{BH}z}) = +1$) and the triangles pointing downwards indicate a change ($\text{sign}(J_{\text{BH}z}) = -1$). As seen, the change indeed happens right near $(r_p/a_0)_{\text{plateau}}$ where $e_{\text{fin}} \approx 1$. We note here that a similar orbital-flip effect has been observed in the Lidov-Kozai case [e.g. 92, 93]. To get a better view of the dynamics, we now consider the top plot in Fig. 5, which shows how the flip occurs using a full three-body integration of the problem. The solid lines show the orbits of the two BHs in their COM, where blue lines highlight their evolution before the orbital flip ($\text{sign}(J_{\text{BH}z}) = +1$) and the orange lines after the flip ($\text{sign}(J_{\text{BH}z}) = -1$). As seen, the flip occurs on a timescale that is less than the initial orbital time of the BBH, denoted by T_0 , and therefore represents a ‘non-adiabatic maneuver’. This leads us to another important point, namely that even though the BBH changes orbital spin direction, it does not generally lead to a prompt merger during the flip, although the BBH angular momentum is able to vanish right in the flip (depending on the orbital configurations). In other words, the so-called osculating elements of the BBH $a, e, r_{\text{BH}} = a(1-e)$ might predict that $r_{\text{BH}} \approx 0$ during the flip which would lead to a prompt merger; however, as the flip does not happen adiabatically, but instead almost promptly in less than one orbit, the BBH is most likely never to pass through the peri-center passage $r_{\text{BH}} \approx 0$ as otherwise suggested by the osculating elements. This point is illustrated in the bottom plot of Fig. 5, which shows the actual distance between the two BHs in the binary, $|\mathbf{r}_1 - \mathbf{r}_2|$, and the osculating peri-center distance, $r_{\text{BH}} = a(1-e)$, as a function of time. As seen, right at the flip near $t/T_0 \approx 0$, the osculating value $r_{\text{BH}} = a(1-e)$ suggests the two BHs (or stars) will undergo an extremely close passage that might lead to a merger; however, the real distance $|\mathbf{r}_1 - \mathbf{r}_2|$ shows that they (in this example) never get any closer than their initial peri-center distance. Therefore, one has to be very careful when using orbital average quantities, such as osculating elements, for estimating possible mergers during an interaction.

D. Sign Reversal

The last classical effect we discuss is how a BBH through a weak secular encounter can end up with an eccentricity change Δe that has an opposite sign to what the FO estimate predicts; a feature we denote as ‘sign reversal’. An example of this is shown in Fig. 5. As seen in the middle plot showing the BBH eccentricity as a function of t/T_0 , the BBH’s e first increases from $e_0 = 0.99$ to about $e \approx 0.995$, after which the orbit flips (indicated by blue to orange color) and the eccentricity rapidly decreases and settles at an $e_{\text{fin}} \approx 0.9775 < e_0$. The FO estimate completely breaks down in this limit and predicts a positive Δe of ≈ 0.046 , where the true change is in fact negative, $\Delta e \approx -0.012$. In this partic-

ular example, where the BBH both undergoes an orbital flip and ‘exceeds’ the $e = 1$ limit according to FO theory, the BBH actually ends up with an $e_{\text{fin}} < e_0$ implying its GW inspiral life time τ increases as a result of the encounter; something that is far from clear when considering FO theory only. In comparison, our SO estimate from Eq. (6) predicts a change of $\Delta e \approx -0.005$, which correctly is negative, but slightly off as the initial value of $r_p/a_0 = 3.0$ is close to where the secular approximation breaks down. Indeed, we find in this case that the exact Δe depends on the initial angular phase of the BBH, which is a clear indication of a secular breakdown.

How and for what r_p/a_0 a BBH undergoes a Δe sign reversal can e.g. be seen in Fig. 4 in the top plot, where the full (empty) symbols indicate $\text{sign}(\Delta e) = +1$ ($\text{sign}(\Delta e) = -1$). The locations of sign reversal are also clearly visible in the middle plot, where the crossing between a solid line (e_{fin}) and its corresponding dashed line (e_0) indicates the location where $\Delta e = 0$. For example, a BBH with an $e_0 = 0.99$ that undergoes a weak encounter with $r_p/a_0 \lesssim 3.5$ will end up with a final eccentricity $e_{\text{fin}} < e_0$, and vice versa. As explained, FO theory is not able to resolve any features related to neither the observed ‘plateau’ nor the ‘ Δe sign reversal’; however, our SO theory actually predicts an elegant and simple relation between the location of the plateau, $(r_p/a_0)_{\text{plateau}}$, and the location of sign reversal, $(r_p/a_0)_{\Delta e=0}$. As shown in HS19 the two are related by,

$$\frac{(r_p/a_0)_{\text{plateau}}}{(r_p/a_0)_{\Delta e=0}} = 2^{2/3}, \quad (9)$$

that is, they are universally connected by the simple factor $2^{2/3} \approx 1.59$. Finally, if we consider the functional form of $|\Delta e|$ for $(r_p/a_0) < (r_p/a_0)_{\Delta e=0}$ we see that it has a different power law slope than the classical FO prediction $-3/2$. As described in HS19, the slope is different as this is the region where the SO term from Eq. (6) dominates the change in eccentricity. This explains why the slope is observed to be -3 as this is exactly the slope associated with $e^2 \propto (r_p/a_0)^{-3}$.

E. Post-Newtonian Effects

We end this section by discussing the effects from including PN corrects in the weak interaction itself. PN corrections have been shown to be very important to include for modeling mergers in the strong interaction few-body problem [e.g. 55, 59], and have likewise been shown to play a crucial role in the hierarchical Lidov-Kozai problem [e.g. 94]. The question is how important PN corrections are for our weak interaction scenario. In general, General Relativistic (GR) effects in the PN formalism can be divided into two different groups: conservative and dissipative corrections. We discuss both of these in the following subsections.

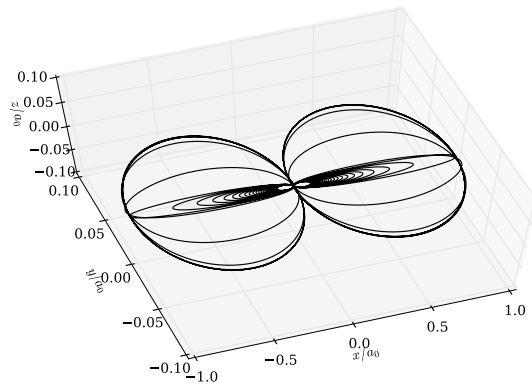


FIG. 6. Orbital evolution of a BBH undergoing a GW inspiral during a single weak encounter. The initial conditions are: $r_p/a_0 = 5.3$, $a_0 = 0.5$ AU, $e_0 = 0.99$, and $i = \pi/2$, $\Omega = -\pi/4$, $\omega = 0$. The simulation only includes the 2.5PN term, as the lower 1,2PN terms lead to precession which make initial conditions ill-defined; however, similar inspirals form with the 1,2PN terms included. When comparing to Fig. 4, one sees that our chosen initial conditions are very close to the plateau described in Section II C. In other words, the weak encounter leads here to a change $\Delta e \approx 1 - e_0$, which leads to a final eccentricity of $e_{\text{fin}} \approx 1$. In this example, the induced GW inspiral time is similar to the time it takes for the encounter to pass the BBH, which explains why we see the BBH clearly beginning its inspiral during the encounter. This illustrates that prompt GW inspirals easily can form from distant weak encounters. Because of its short inspiral time, the BBH will appear near the region in-between the LISA and LIGO bands, i.e. near DECIGO, with notable eccentricity. Further discussions are found in Section II C and II E.

1. Conservative Terms: Precession and Shielding

The conservative corrections, which are represented by the 1,2 PN terms, lead to orbital precession. In our case, including precession in the formalism gives rise to at least two notable effects. The *first effect* is that the initial set of orbital angles (see e.g. Fig. 1), and especially Ω , are no longer staying constant as the perturber moves in from infinity due to precession, and a unique outcome is therefore no longer given by only the classical set of ICs. For a well-defined and unique outcome when PN precession is included, one has to specify exactly where the incoming perturber is for a given set of orbital angles. This also implies that integrating from time $t \in \pm\infty$ for analytically deriving Δe is not possible as one otherwise does in the Newtonian case (HS19). For evolving BBHs in clusters this issue of ‘ill-defined’ classical ICs is not a real problem, as the change in angles from PN precession will be randomized anyway for isotropic random interactions. The *second effect* appears in configurations where the time it takes for the BBH to precess one full 2π orbit due to PN apsidal precession [e.g. 95],

$$T_{1\text{PN}} \approx \frac{T_0}{3} \frac{a_0}{\mathcal{R}_m} (1 - e_0^2), \quad (10)$$

where \mathcal{R}_m denotes the Schwarzschild radius of a BH with mass m , is shorter than the time scale it takes for the encounter to pass the BBH, a time we here refer to as the peri-center passage time T_3 ,

$$T_3 \approx \sqrt{\frac{r_p^3}{Gm}}, \quad (11)$$

where we have omitted terms of order unity. In such cases, the interaction is no longer simply described by an incoming single interacting with a BBH on a closed Keplerian orbit, as the one illustrated in Fig. 1, but instead by a single interacting with a ‘disc’ build up by ‘rosetta’ orbits with inner and outer annuli equal to the BBH’s peri-center and apo-center, respectively. This symmetry change from a non-axisymmetric closed orbit to an axisymmetric disc is expected to ‘shield’ the BBH from perturbations, in the same way as a circular BBH is much harder to perturb than an eccentric [e.g. 87]. Using the above equations (10) and (11), one finds that such shielding will start to appear for encounters satisfying the following inequality,

$$\begin{aligned} \frac{r_p}{a_0} &\gtrsim \frac{a_0^{2/3}}{\mathcal{R}_m^{2/3}} (1 - e_0^2)^{2/3} \\ &\gtrsim 10^3 \times \left(\frac{a_0}{0.5\text{AU}}\right)^{2/3} \left(\frac{m}{20M_\odot}\right)^{-2/3} \left(1 - (e_0/0.99)^2\right)^{2/3}, \end{aligned} \quad (12)$$

where we again have omitted factors of order unity. As seen, even for BBHs with initial high eccentricity, corrections from PN precession are likely not to play a significant role. However, one might still find resonant couplings between the precession and encounter frequencies for lower values of r_p/a , which could lead to PN precession corrections. We do not have the necessary analytical tools to quantify these highly interesting effects yet, but we will follow up on this in upcoming work. Also, for this work we updated our PN code to also include the 1,2PN terms, but as also noticed in [67], it is numerically challenging to evolve highly relativistic and eccentric BBHs with these corrections.

2. Dissipative Terms: Prompt GW Inspiral

The dissipative corrections, which first appear at the 2.5PN order, lead to orbital decay for a BBH, which will result in a merger if its eccentricity is high enough for its GW inspiral life time to be shorter than its dynamical disruption time. As described in Section II C, a BBH can be driven to a very high eccentricity e by weak encounters near the plateau, and can in principle reach $e \approx 1$ during orbital flips. The question is what happens to such interactions when dissipative corrections, here included by the 2.5 PN term, are included. An example is shown in Fig. 6, which shows the orbital evolution of a BBH over the duration of a weak encounter for an interaction near the

plateau. As seen, the weak encounter drives the BBH to such a high eccentricity that the 2.5PN correction term starts to take over the evolution, which leads to a clear orbital decay during the interaction. The inspiral time of such binaries are of order the peri-center passage time of the encounter w.r.t. the COM of the BBH, which interestingly fills in the ‘gap’ in GW peak frequency space between the 3-body mergers and 2-body mergers studied in [55] and later discussed in Section III B 3. Note here that Fig. 6 shows results for a BBH that is similar to the one shown in Fig. 5, the only difference is that the one considered in Fig. 6 undergoes a weak encounter from further away; GR effects are therefore not generally associated with only close strong and weak interactions, but can play a significant role for even very distant perturbers. Finally, in Fig. 4 results from including the 2.5PN term in weak interactions are shown with *black symbols*, where no symbol for the upper two figures, and a cross symbol in the bottom plot, indicates the BBH merged during the weak interaction. As seen, for interactions where the BBH do not merge during the interaction the final outcomes are similar to the ones derived using Newtonian dynamics alone. For interactions where the BBH does merge during the interaction, we find notable differences when including the 2.5PN term in especially the final inspiral time, as seen in the bottom plot. As pointed out in the above paragraph, such mergers can lead to distinguishable peaks in GW peak frequency space, and are therefore in general important to keep track of.

3. Summary

To conclude, including the 2.5PN dissipative correction is easy and gives rise to potentially important and interesting prompt GW inspiral mergers forming during or right after the weak interaction. The conservative 1,2PN corrections are more difficult to include in the problem, as they also often lead to numerical challenges in the relevant regimes where the 2.5PN correction is also important. The 1,2PN terms can lead to shielding effects that protect the binary from changing eccentricity for very distant encounters; however, using simple scaling arguments, we have proven that this correction is likely not to play a significant role for astrophysical cluster BBHs, but we will study this in further detail in an upcoming paper. For these reasons, all our studies later on in this paper are based on including the 2.5PN term alone.

III. BLACK HOLE BINARIES IN CLUSTERS

Having addressed in the above Section II the outcome of a single weak interaction, we now turn to the question of what the outcome is of a BBH undergoing a series of weak and strong binary-single interactions inside a dense cluster.

BBHs in dense clusters can be driven to merger during their dynamical hardening through few-body interactions such as binary-single [59] and binary-binary [66] interactions. Following [55], and later described in Section III A 2, we refer to a BBH that merges during a strong binary-single interaction by a *3-body merger*, and a BBH that merges in-between its strong interactions by a *2-body merger*. As further described in [55] and [47], such mergers can only form if their GW inspiral time is less or comparable to the characteristic dynamical time of their associated interaction channel, which for 3-body mergers is ~ 1 year (characteristic orbital time of a BBH in a typical GC), and for 2-body mergers is 10^7 years (characteristic time for a BBH to undergo its next strong encounter in a typical GC). These characteristic time scales directly maps to how the merging BBHs distribute in GW peak frequency f_{GW} and orbital eccentricity e . Following [64], the value of f_{GW} for a BBH with peri-center distance r_{BH} can be approximated by the GW frequency found from assuming the BBH is circular with a SMA equal to r_{BH} . From using that the emitted GW frequency is two times the Keplerian orbital frequency one now finds,

$$f_{\text{GW}} \approx \frac{1}{\pi} \sqrt{\frac{2Gm}{r_{\text{BH}}^3}}. \quad (13)$$

In [56] it was illustrated that a BBH that has to inspiral on a time scale \mathcal{T} , will have an f_{GW} equal to

$$\frac{f_{\text{GW}}}{\text{Hz}} \approx 2 \cdot 10^{-5} \left(\frac{\mathcal{T}}{10^{10} \text{yrs}} \right)^{-3/7} \left(\frac{a}{0.5 \text{AU}} \right)^{3/14} \left(\frac{m}{30 M_{\odot}} \right)^{-11/14} \quad (14)$$

From this relation one concludes that 2-body mergers with $\mathcal{T} \sim 10^7$ years will form near the LISA band, where 3-body mergers with $\mathcal{T} \sim 1$ year form near the LIGO band. As pointed out in [55] and [56], these dynamically formed BBH populations will therefore leave unique observational imprints across the LISA, DECIGO and LIGO bands, which can be used to probe their dynamical history and astrophysical origins. This is highly interesting and encouraging; however, what has not been discussed in these recent studies is the effect from weak interactions, and their possible importance for an accurate modeling of the observable f_{GW} and e distributions. We address this question in this section.

A. Post-Newtonian Cluster Model

In this section we start by introducing our cluster model, and how we keep track of different GW merger outcomes. We then describe in simple words the routines of our MC cluster algorithm, and especially how we include the effects from both GW emission, and strong

and weak interactions¹. In the last part we present our main results on the role of weak interactions using our introduced MC cluster algorithm.

1. Strong Interactions and Dynamical Ejection

For modeling BBH mergers forming in clusters including weak and strong interactions, we make use of the following simple model inspired by [55]. We consider a BBH that starts out with an initial SMA a that is slightly below the hard-binary (HB) value given by

$$a_{\text{HB}} \approx \frac{3 Gm}{2 v_{\text{dis}}^2}, \quad (15)$$

We imagine this BBH lives in a population of single BHs, all with the same mass m , characterized by a constant number density n_s , velocity dispersion v_{dis} , and escape velocity v_{esc} . The BBH will undergo both strong and weak interactions defined in the following way: We denote an interaction a *strong interaction* if the incoming single BH passes the BBH on an orbit with peri-center distance $r_p < \mathcal{C}a$, where our fiducial value of \mathcal{C} is here $\mathcal{C} = 2$, and a is the SMA of the BBH at the time the single passes the BBH. An interaction with $r_p > \mathcal{C}a$ will instead be labeled a *weak interaction*. We assume that each strong interaction leads to a constant decrease in the SMA of the BBH from a to a_{enc} as,

$$a_{\text{enc}} = a \times \delta, \quad (16)$$

where we use $\delta = 7/9$, which equals the average value assuming the chaotic binary-single interaction can be modeled by an ergodic distribution as discussed in [64]. At the same time we assign the BBH a new eccentricity e that is drawn from a so-called thermal distribution $P(e) = 2e$ [78]. We choose this simple model for strong interactions due to the following three reasons. (i) It provides full analytical solutions to both the stationary BBH population [e.g. 96] and the highly eccentric evolving population across all GW bands [e.g. 47, 64]. This allows us to not only cross check all our algorithms, but also to extract small changes coming from additional terms such as weak interactions. (ii) The simple δ -model has been used in all our previous studies, which allows for an easy comparison. Despite its simplicity, our previous results [e.g. 55] are in surprisingly good agreement with more sophisticated MC techniques [e.g. 57]. (iii) Adding weak interactions into the evolution of BBHs requires in principle large computational resources, as weak interactions need to be performed $\gg 1$ times in-between each strong interaction. Therefore, partly due to computational limitations, we restrict ourself to our simple δ -model combined

¹Our developed code is free to use, and can be obtained by contacting the lead author of the paper.

with additional hybrid techniques, as described later.

This process of a gradual decrease of the BBH's SMA is loosely referred to as *hardening*. In the point-particle Newtonian limit this will always end with a dynamical ejection of the BBH when its SMA reaches the following critical value,

$$a_{\text{ej}} \approx \frac{1}{6} \left(\frac{1}{\delta} - 1 \right) \frac{Gm}{v_{\text{esc}}^2}, \quad (17)$$

which is where the recoil velocity from the 3-body interaction equals the escape velocity of the cluster [64]. This classical hardening process therefore leads to an ejection of BBHs with a SMA $\sim a_{\text{ej}}$ and an eccentricity distribution that is thermally distributed. As shown by [19, 24], this population of ejected BBHs can explain at least part of the observed LIGO merger rate, but as pointed out by e.g. [55, 64], this picture is highly incomplete as it only includes (energy conserving) Newtonian dynamics. This is described in greater detail below.

2. Energy Dissipation and Few-body Mergers

When GR dissipative terms – where the leading term is the 2.5PN term in the PN expansion formalism – are included in the dynamics, a BBH can also merge inside its cluster either *during* or *in-between* its strong interactions. We describe our methods for modeling these outcomes in the following paragraphs.

3-body Mergers: For determining if a BBH merges during a strong 3-body interaction, we model this often highly chaotic and resonating state using the approach put forward in [64]. The interaction here is divided up into N_{IMS} intermediate states (IMSs), each of which is described by a BBH with a bound single BH. For each IMS we assign the corresponding BBH an eccentricity sampled from the thermal distribution $P(e) = 2e$, but keep the SMA fixed to its initial value a_0 . To determine if the BBH undergoes a GW inspiral merger during this IMS, i.e. merge while the third objects is still bound to it, we compare the energy radiated over one orbit of the BBH,

$$\Delta E_{\text{GW}} \approx (85\pi/12)G^{7/2}c^{-5}m^{9/2}r_{\text{BH}}^{-7/2}, \quad (18)$$

to the total orbital energy of the bound 3-body state,

$$E_{\text{B}} \approx Gm^2/(2a_0). \quad (19)$$

If $\Delta E_{\text{GW}} > E_{\text{B}}$ we label the IMS assembled BBH as a 3-body merger. This energy threshold is equivalent of saying that the BBH will undergo a GW inspiral merger during the interaction if its peri-center distance $r_{\text{BH}} < r_{3\text{cap}}$, where $r_{3\text{cap}}$ is a ‘3-body capture distance’ given by [64],

$$r_{3\text{cap}} \approx \mathcal{R}_m \times (a_0/\mathcal{R}_m)^{2/7}. \quad (20)$$

If instead $r_{\text{BH}} > r_{3\text{cap}}$ the BBH does not merge during the considered IMS. We repeat this process, i.e. first assign the IMS assembled BBH an eccentricity from $P(e) = 2e$ and then compare its r_{BH} to $r_{3\text{cap}}$, up to $N_{\text{IMS}} = 20$ times per interaction, which is the average number of IMSs assembled in a chaotic equal mass 3-body interaction [64]. The total probability for a BBH to merge during a 3-body interaction, $P_{3\text{m}}$, i.e. to be formed with orbital parameters such that $r_{\text{BH}} < r_{3\text{cap}}$, can in this model be expressed analytically as follows [64],

$$P_{3\text{m}} \approx \frac{2r_{3\text{cap}}}{a_0} \times N_{\text{IMS}}. \quad (21)$$

As illustrated in [64], by integrating this probability up over a BBHs hardening binary-single interactions from a_{HB} to a_{ej} , one finds that the total probability for a BBH to merge during a 3-body interaction relative to merging outside the cluster within a Hubble time is $\approx 10\%$.

2-body Mergers: For keeping track of the formation of 2-body mergers, we evolve the orbital parameters a, e of the BBH in question in-between each interaction according to the equations given by [90]. If at any given time the GW inspiral life time of the BBH right after it has finished an interaction, τ , is less than the time it takes before it undergoes its next interaction, t_{int} , we stop the code and label the outcome a 2-body merger. To calculate the time before the next interaction, we use the same approach as for Eq. (4). Assuming that we keep track of single encounters up to a maximum peri-center distance of R_{p} , the time in-between interactions can be approximated by,

$$t_{\text{int}} \approx \frac{1}{6\pi G} \frac{v_{\text{dis}}}{n_{\text{s}} m R_{\text{p}}}. \quad (22)$$

As argued in Section II B, one does expect the results to converge for R_{p} going to infinity. We will address this issue later in Section III B 3.

3. BBH Evolution with Weak Interactions

We now describe our numerical scheme used in this paper for modeling the evolution of BBHs inside a dense stellar cluster with the inclusion of weak interactions. It expands on a similar model put forward by [47, 55, 64].

We start by first choosing the maximum relative peri-center distance within which we model the effect from interactions, R_{p}/a , where a is the SMA of the BBH in question. This rescaled value stays constant, but the physical value of R_{p} will decrease as the BBH hardens inside its cluster. If only strong interactions are included, then $R_{\text{p}}/a \sim 1$. Therefore, a value of $R_{\text{p}}/a \gg 1$ will allow the orbital parameters of the BBH to be affected by a much wider and numerous range of interactions compared to the previously studied strong interaction case. With this choice of R_{p}/a , we follow the evolution of a BBH from its initial SMA, $a_{\text{in}} \sim a_{\text{HB}}$,

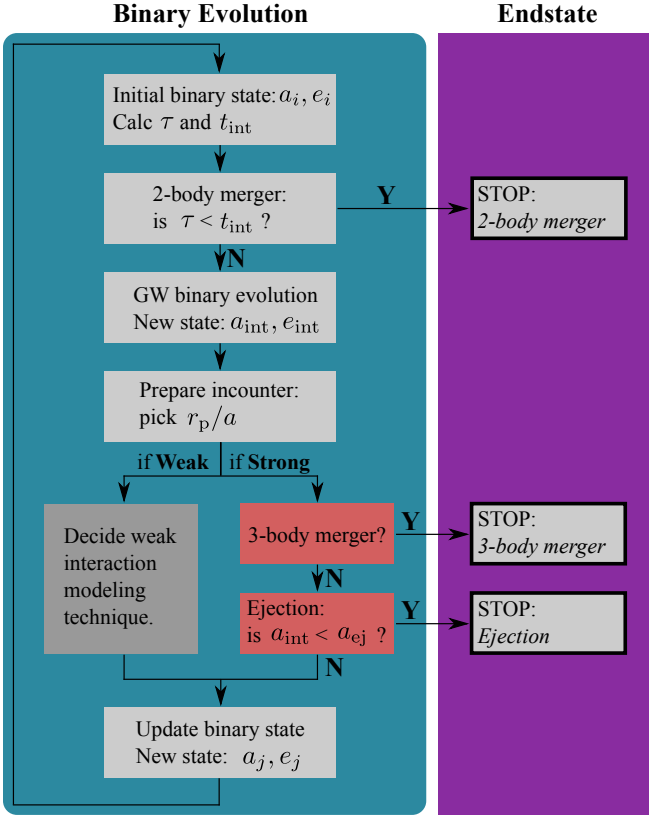


FIG. 7. Flowchart illustrating the main steps and logic of our BBH evolution algorithm described in Section III A 3. The left *blue box* evolves the BBH from state i to state j , which includes GW and dynamical evolution. Based on what value that is picked for the peri-center distance of the incoming single w.r.t. the BBH COM, r_p/a , the interaction is described either by a weak (if **Weak**) or a strong interaction (if **Strong**). The right *purple box* highlights the three main endstates we keep track of: 2-body merger, 3-body merger, and dynamical ejection. The flowchart only shows the most important steps of our routine, and includes therefore not additional stopping criteria such as BBH merger forming during a weak interaction; however, our full procedure is described in detail in Section III A 3.

towards its final value, $a_{\text{fin}} \sim a_{\text{ej}}$, assuming all properties of the cluster stay constant. As R_p/a takes a finite value we are able to evolve the BBH in finite steps. In the following we describe how we evolve the BBH from step i to its next step j . See also Fig. 7 which shows a simplified flowchart of our algorithm.

(1) Check for 2-body merger: Based on the BBH’s orbital values at step i , referred to as $\{a_i, e_i\}$, and the value of R_p/a , we first derive τ and t_{int} using Eq. (3) and (22), respectively. If $\tau < t_{\text{int}}$ we stop the code and record the BBH as a 2-body merger. If instead $\tau > t_{\text{int}}$, we proceed as follows.

(2) GW orbital evolution: If no 2-body merger has occurred, we evolve the BBH’s orbital parameters

using the equations from [90] over the time interval it takes for it to undergo its next encounter t_{int} . During this evolution the orbital parameters of the BBH evolve from $\{a_i, e_i\}$ to $\{a_{\text{int}}, e_{\text{int}}\}$.

(3) Pick encounter distance: We now prepare for the encounter. For this we start by randomly picking a peri-center distance for the encounter w.r.t. the COM of BBH, r_p/a_{int} , in the range $[0 : R_p/a_{\text{int}}]$ assuming the encounters are isotropically distributed at infinity (see e.g. [59]). At this step we just record the value r_p/a_{int} .

(4) Classify and perform encounter: At this step we start by classifying the encounter type from the above step. We do this as follows.

- *Strong Interaction:* If $r_p/a_{\text{int}} < \mathcal{C}$, we model the interaction as a strong interaction. To evaluate the corresponding outcome we first estimate if the interaction results in a 3-body merger using the IMS-decomposition approach described in Section III A 2. If a 3-body merger does not form, we model the interaction outcome using our simple δ -model described in Section III A 1. If at this point $a_{\text{int}} < a_{\text{ej}}$, we stop the code after the interaction and record the BBH as being ejected from the cluster.

- *Weak Interaction:* If instead $r_p/a_{\text{int}} > \mathcal{C}$, we model the interaction as a weak interaction. For this we start by picking a random configuration for the angles $\{i, \omega, \Omega\}$ assuming an isotropic distribution. We then derive the outcome using one of the following ways. (i): Use our few-body code described in [85]. (ii): Use our SO result from Eq. (6). (iii): Use a ‘hybrid approach’ where we combine (i) and (ii). As discussed later, option (i) is numerically challenging, but straight forward. Option (ii) is in-accurate for $r_p/a_{\text{int}} \sim \mathcal{C}$, but extremely fast. Therefore, option (iii) is often the best option, but it requires bridging (i) and (ii).

- *Final parameters:* If the BBH has not merged at this point its final set of orbital values will be $\{a_j, e_j\} = \{a_{\text{int}} + \Delta a, e_{\text{int}} + \Delta e\}$, with Δa and Δe derived as just described.

(5) Next step and termination: For a BBH that has survived all interactions and is still inside the cluster, we end this ‘one interaction’-routine from step i to j by simply putting $\{a_j, e_j\} \rightarrow \{a_i, e_i\}$. After this we go back to the start and repeat the process. We keep doing this until the BBH either merges inside the cluster or is ejected.

Using this algorithm we can quickly build up a distribution of BBH properties showing e.g. the distribution of BBH eccentricity e across different f_{GW} bands from LISA to LIGO. Our model does represent a simplified picture of how BBHs undergo dynamical interactions in dense stellar systems; however, our extremely fast approach has shown to give surprisingly accurate predictions for how BBHs merge and distribute across both f_{GW} and e . Our model can easily be improved,

but its simplicity as well as its corresponding list of available analytical solutions makes it an ideal testbed for including new effects, as the ones we consider in this paper. Below we study outcomes from this model.

B. Results from Including Weak Encounters

In this section we present our main results for how BBHs interact and merge in clusters under the influence of both weak and strong interactions. After defining our fiducial parameters and approach below, we study the dynamical history of a single BBH. After this we move to results derived from a large sample of evolved BBHs using MC techniques, from which we derive f_{GW} and e distributions relevant for especially LISA. As illustrated, we find clear observational differences when weak interactions are included.

1. Fiducial Parameters

In all our models we use the algorithm described in the above Section III A 3. If not stated otherwise, we further assume the following set of ‘fiducial model’ parameters: $m = 20M_{\odot}$, $n_s = 10^5 \text{ pc}^{-3}$, $v_{\text{dis}} = 10 \text{ kms}^{-1}$, $v_{\text{esc}} = 50 \text{ kms}^{-1}$, $R_p/a = 50$, and $\mathcal{C} = 2$. These are chosen for easy comparison to previous work. For our main results presented below, we also employ the following ‘hybrid approach’ for accurate and fast modeling of the outcome from weak encounters: for encounters with $2 < r_p/a < \max(5, (r_p/a_0)_{\text{FO}}^{\text{BR}})$ we use a full 2.5PN three-body integration to evaluate the outcome, where for $r_p/a > \max(5, (r_p/a_0)_{\text{FO}}^{\text{BR}})$ we use HS19 given by Eq. (6). In Section III C we compare results from this hybrid approach to results using HS19 only.

2. A Single Black Hole Binary

We start by studying the evolution of a single BBH undergoing both weak and strong encounters inside a dense cluster. Results are presented in Fig. 8, which shows in the top, middle, and bottom plots the BBH’s eccentricity e , the value of r_p/a_0 , and the BBH’s peak GW frequency f_{GW} , respectively, as a function of the number of scatterings, N_{sc} (scattering counter). For this modeling we have used our numerical scheme described in Section III A 3, with the hybrid approach and fiducial cluster parameters listed in the above Section III B 1.

As seen, the BBH occasionally undergoes notable evolution in eccentricity in-between its strong interactions (red crosses). For example, the BBH evolves from an eccentricity of ~ 0.8 to ~ 0.9 over the range $N_{\text{sc}} \approx 400\text{--}500$ entirely through weak interactions (grey dots). A relevant question is here if weak interactions therefore are expected to lead to an observed eccentricity distribution that is notably different from the thermal distribu-

tion that often follows from strong scatterings. However, by studying a large number of runs of BBHs evolving through both weak and strong interactions, we did not find any significant differences when weak interactions are included. We will however study this in more detail in an upcoming paper. See also [89] for a similar analysis.

The importance of including weak encounters becomes clear when considering the end of the evolution of the BBH shown in Fig. 8. As seen, the last strong interaction leaves the BBH with an eccentricity of $e \approx 0.9$, which is not even high enough for it to merge before its next strong interaction (if the BBH has an inspiral time $\tau < t_{\text{SE}}$, where t_{SE} is the time interval before the next strong encounter (see Eq. (4)), the state is marked with a grey diamond). However, the BBH is instead driven to merge entirely through weak interactions, each of which changes the BBH’s eccentricity until $\tau < t_{\text{int}}$. This evolution also brings the BBH into the LISA band, as seen in the bottom plot, which will make it appear as a high eccentricity LISA source. Such eccentric sources are not a natural outcome of isolated BBH evolution, and therefore provide a test of the cluster channel [55, 57].

Finally, the top plot shows how the analytical estimates HR96 (green circles), and HS19 (blue circles), compare to our full numerical results (black dots). As seen, both HR96 and HS19 provide excellent estimates when $r_p/a \gg 1$; however, both start to break down, as expected, when approaching the strong interaction limit. The important difference between HR96 and HS19 is seen for BBHs that scatter around the $e \approx 1$ limit. For example, HR96 clearly gives rise to several unphysical outcomes with $e > 1$ when the BBH is already highly eccentric; a problem that is resolved by using HS19 due to its corrections from the SO term. The high eccentricity region is the most interesting and relevant for understanding and modeling how BBHs are driven to merge, which again illustrates the importance of using corrections similar to the one encoded in HS19.

3. A Population of Black Hole Binaries

We now turn to the study of what GW signals to expect from a population of BBHs evolving through weak and strong interactions, similar to the population that we potentially observe from GCs throughout the nearby observable universe. For this, we here model the dynamics of an ensemble of 15000 individual BBHs, and follow their evolution in a similar way as the one described in the above Section III B 2. We record 2-body and 3-body BBH mergers, as well as properties for the ejected BBH population. From this data we derive f_{GW} and e distributions, as described in the following sections. In this sub-section all our results are based on the fiducial values and hybrid approach outlined in Section III B 1.

We first consider Fig. 9, which shows the distribution of f_{GW} (top plot) and the eccentricity distribution at 10^{-2} Hz (bottom plot) of the merging BBH popula-

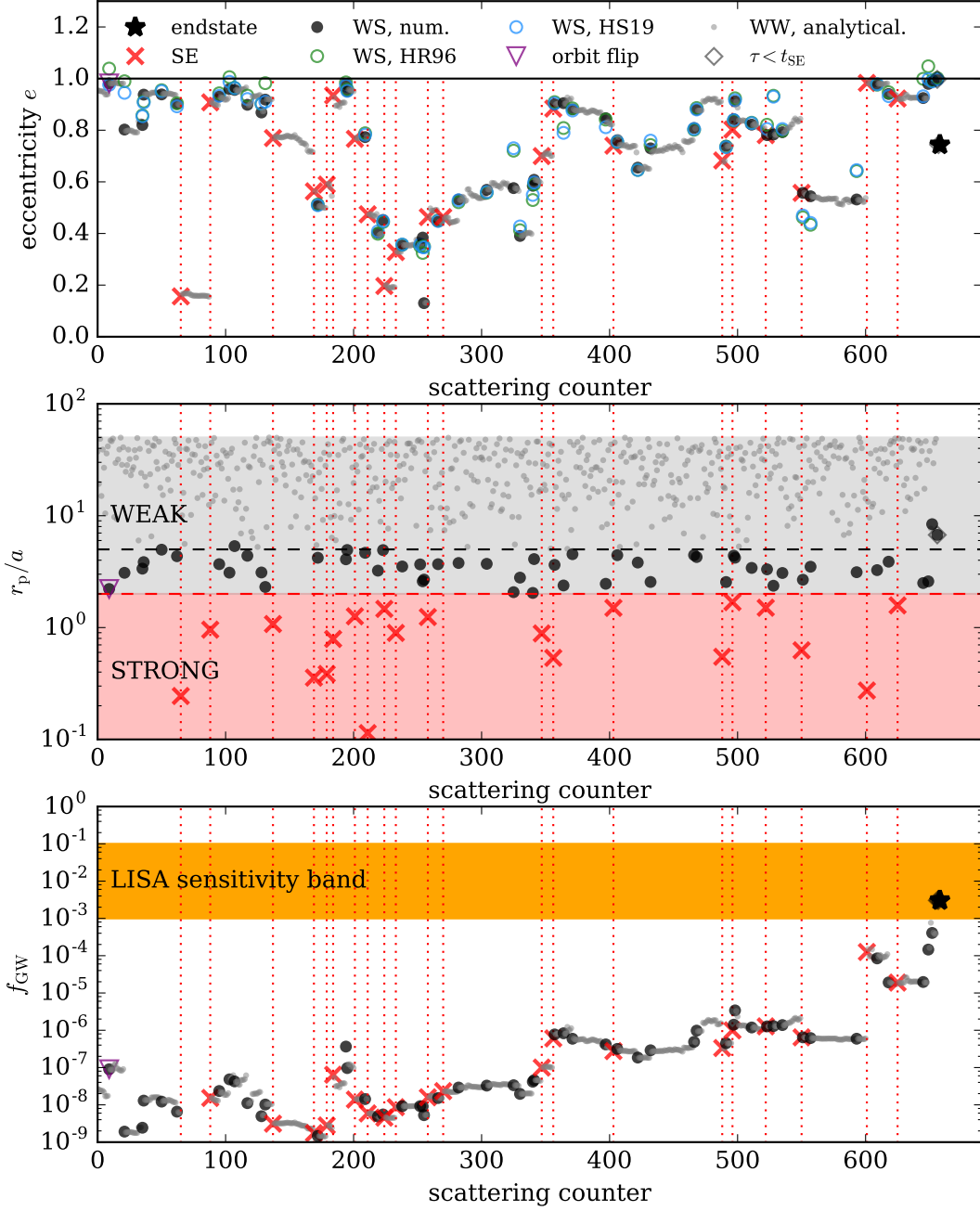


FIG. 8. Dynamical history of a BBH evolving inside a cluster through equal mass weak and strong three-body interactions. For this simulation we have used our numerical scheme outlined in Section III A 3, with the inclusion of the following hybrid approach as further described in Section III B 2. In short: For *strong encounters* (SE), characterized here by $r_p/a < 2$, we evolve the BBH assuming the SMA $a \rightarrow \delta a$, and $P(e) = 2e$. For *weak-strong encounters* (WE), characterized here by $2 < r_p/a < 5$, we use our 2.5PN code to evaluate the outcome. For *weak-weak encounters* (WW), characterized here by $r_p/a > 5$, we assume $\Delta a = 0$ and use Eq. (6) to derive Δe . For the whole evolution we use the fiducial cluster values listed in Section III B. The BBH evolves from its initial values from left to right as a function of scatterings (scattering counter), and ends by merging inside the cluster in-between its interactions (2-body merger). Each point in the plots shows the resulting outcome from the corresponding scattering. We use the following labeling to highlight different encounters and outcomes: *Red cross*: Strong-encounter (SE). *Black dot*: Weak-strong encounter (WS); result from our numerical integration. *Green circle*: Weak-strong encounter (WS); result from HR96. *Blue circle*: Weak-strong encounter (WS); result from HS19. *Purple triangle*: BBH orbital flip. *Grey dot*: Weak-weak encounter (WW). *Grey diamond*: The BBH’s inspiral time, τ is $<$ than the time it takes for the next strong encounter to happen, t_{SE} . *Black star*: Endstate; at this point the BBH will inspiral in near isolation with no further perturbations ($\tau < t_{int}$). Each of the *red dotted* vertical lines indicate a SE; evolution in-between these lines is therefore due to weak encounters and GW emission only. The *top plot* shows the BBH’s eccentricity e . The *middle plot* shows r_p/a for each scattering, with weak and strong scattering zones highlighted (grey/red). The *bottom plot* shows f_{GW} with the LISA band overlotted. Results are discussed in Section III B 2.

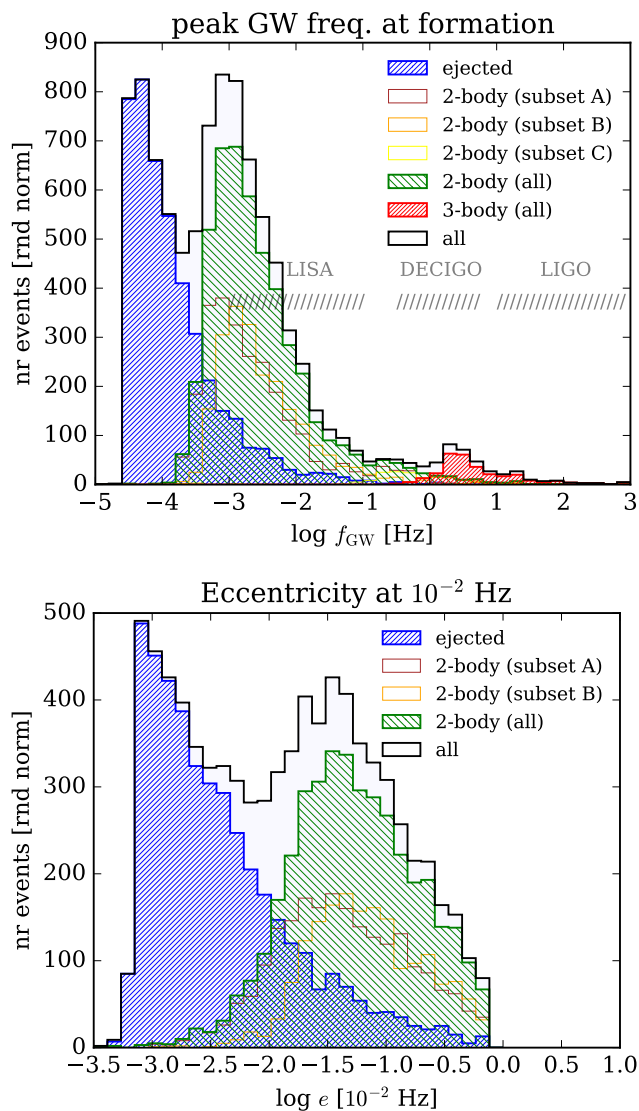


FIG. 9. Distribution of GW peak frequency f_{GW} (*top plot*), and BBH orbital eccentricity evaluated at $f_{\text{GW}} = 10^{-2}$ Hz (*bottom plot*), derived from 15000 individual runs of BBHs undergoing weak and strong scatterings inside a dense cluster. For this, we used the numerical scheme outlined in Section III A 3, using our ‘fiducial cluster parameters’ and ‘hybrid approach’ described in Section III B. The distributions are divided into the following sub-categories: *Ejected*: BBHs ejected from the cluster with an inspiral time $\tau < t_{\text{H}}$. *2-body (Subset A)*: 2-body mergers where the BBH from the last recorded strong-encounter has $\tau > t_{\text{SE}}$, i.e. the BBH merges due to weak encounters. *2-body (Subset B)*: 2-body mergers where the BBH from the last recorded strong-encounter has $\tau < t_{\text{SE}}$. *2-body (Subset C)*: BBHs that merge during a weak interaction. *2-body (all)*: All 2-body mergers, i.e. subset $A+B+C$. *3-body (all)*: All 3-body mergers. *All*: All mergers, i.e. ejected + 2-body + 3-body. The distribution of f_{GW} is the value at ‘formation’, i.e. right when we identify the BBH in question to either have been ejected, has an inspiral time $\tau < t_{\text{int}}$ for 2-body mergers, or a peri-center distance during a 3-body interaction $r_{\text{BH}} < r_{3\text{cap}}$ for 3-body mergers. Results are discussed in Section III B 3.

tion. As described in the caption, f_{GW} is the GW peak frequency recorded at the time of ‘formation’, i.e. right when either the BBH in question is ejected from the cluster for ejected mergers, $\tau < t_{\text{int}}$ for 2-body mergers, or right when $r_{\text{BH}} < r_{3\text{cap}}$ for 3-body mergers. This distribution is therefore not universal, as t_{int} depends on R_{p} (a higher R_{p} will allow each BBH to inspiral over a longer time scale before the code halts, which will drive the 2-body merger distribution slightly to the right). However, it only weakly depends on R_{p} as each BBH inspirals with near constant f_{GW} , and the plot therefore still provides some useful insight into how the different outcomes distribute and differ from each other. As seen, ejected mergers tend to form below both the LISA and the LIGO bands, and will therefore almost circularize before being observable, whereas 2-body mergers will appear eccentric in LISA, and 3-body mergers in LIGO. As described in [56], and illustrated by Eq. (14), this splitting of outcomes across f_{GW} is linked to the characteristic inspiral times of each population. The bottom plot of e at 10^{-2} Hz is in principle not dependent on R_{p} , as long as the problem converges with increasing R_{p} . From this plot it is clear that the 2-body mergers dominate the population of eccentric sources in the LISA band. The different colored lines in both plots illustrate different dynamical subsets, as described in the figure caption. Starting with comparing *Subset A* (last strong interaction has $\tau > t_{\text{SE}}$, i.e. BBHs are here driven to merger through one or more weak encounters) and *Subset B* (last strong interaction has $\tau < t_{\text{SE}}$, i.e. the BBHs will here still be labeled mergers using a strong interactions code only), we see that there is no major difference between the two. It will therefore generally be hard to tell the difference between strong and weak interaction driven BBH mergers from a few LISA observations alone (in this statement we have ignored rare exotic mergers such as a BBH promptly driven to merger through an interplay between PN corrections and a dynamical flip-orbit during a weak interaction). The only major difference across f_{GW} from the weak interaction channel is the appearance of *Subset C*, which originates from BBHs that merge during the weak encounter (see e.g. Fig. 6). As seen, these mergers appear at relatively high frequencies where they make up their own ‘bump’ slightly below the 3-body mergers.

To systematically explore the role of including weak encounters we now consider Fig. 10, which shows the distribution of f_{GW} (top plot) and the eccentricity e distribution at 10^{-2} Hz (bottom plot), where the *solid black* and *solid red* lines show results from including weak interactions ($R_{\text{p}}/a = 50$) and not including weak interactions ($R_{\text{p}}/a = 2$) in the BBH evolution, respectively. The companion Fig. 11 shows the cumulative distribution of the eccentricity distribution at 10^{-2} Hz from Fig. 10. From considering these figures, one sees that including weak interactions leads to a notable increase in the number of GW sources that will appear with measurable eccentricity ($> 10^{-2}$) in the LISA band. For example, the number of sources with $\log(e) > -1.0$ at 10^{-2} Hz increases by

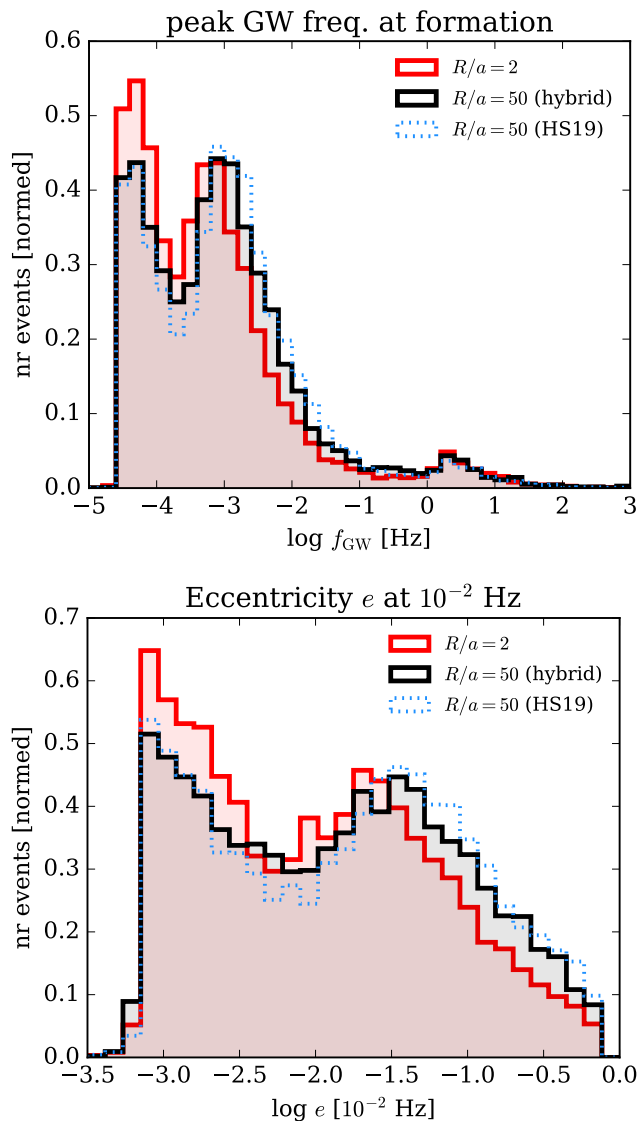


FIG. 10. Distribution of GW peak frequency f_{GW} (*top plot*), and BBH orbital eccentricity evaluated at $f_{\text{GW}} = 10^{-2}$ Hz (*bottom plot*), derived from 15000 individual runs of BBHs undergoing weak and strong scatterings inside a dense cluster. For this, we used the numerical scheme outlined in Section III A 3 and our ‘fiducial cluster values’ listed in Section III B. The *solid red*, *solid black* and *dotted blue* histograms represent the following distributions, respectively. $R_p/a = 2$: Maximum peri-center distance is here set to $R_p/a = 2$, i.e. this set includes strong encounters only. $R_p/a = 50$ (*hybrid*): Maximum peri-center distance is here set to $R_p/a = 50$, i.e. this set also includes weak encounters. To evolve and model each weak encounter we make use of our ‘hybrid approach’ described in Section III B. $R_p/a = 50$ (*HS19*): Similar to $R_p/a = 50$ (*hybrid*), but here all weak interactions are modeled using HS19, i.e. the whole evolution is done using fully analytical prescriptions. As seen, the full analytical approach ($R_p/a = 50$ (*HS19*)) provides a very good estimate compared to the more accurate, but also much slower, hybrid approach ($R_p/a = 50$ (*hybrid*)). Associated cumulative distributions are shown in Fig. 11. Results are discussed in Section III B 3.

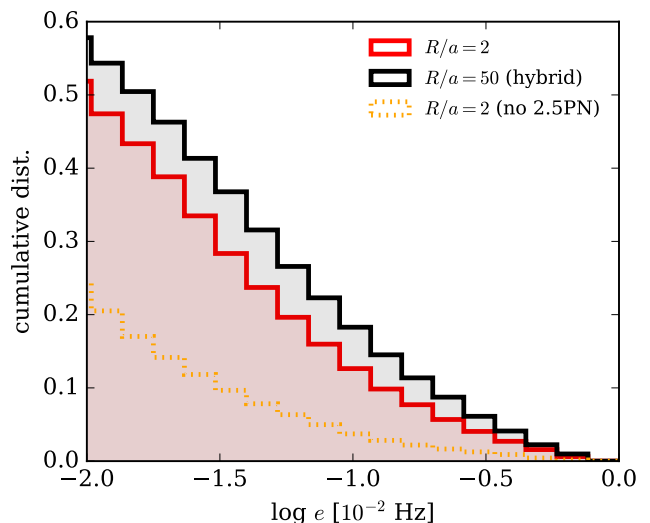


FIG. 11. Cumulative distribution of the bottom plot from Fig. 10. The *solid red* and *solid black* distributions are described in the caption of Fig. 10. The *dotted orange* line shows the result from including strong encounters only and without any 2.5PN corrections, i.e. it shows results from a pure Newtonian strong scattering approach. As seen, for an accurate modeling one needs to include both 2.5PN corrections and weak encounters. In [55, 56] we pointed out for the first time the importance of 2.5PN corrections, here we illustrate the importance of weak encounters.

about $\approx 50\%$. The reason can be found from considering Fig. 12, which shows the number of in-cluster mergers (2-body + 3-body mergers) relative to the number of BBHs ejected from the cluster with $\tau < t_H$, where t_H denotes the Hubble time, as a function of R_p/a . As seen, as more and more weak encounters are included, i.e. as we increase R_p/a , more of the BBHs will merge inside the cluster before being ejected. The increased number of eccentric LISA sources therefore primarily originates from an increase in the number of in-cluster mergers. The corresponding slight systematic shift towards higher e seen in the bottom plot of Fig. 10 for the in-cluster mergers also help increasing the number.

We do not yet have a solid analytical understanding for how the relative importance of weak interactions change with the cluster parameters as we do for strong interactions [e.g. 64]; however, the first results presented here are interesting, and weak interactions definitely add an interesting complexity to the problem. They are also highly important to include for an accurate modeling of possible secular effects on the BBHs if the cluster is not perfectly spherical [97, 98], and might also play a key role in accurately predicting the formation rate of 2. generation mergers [e.g. 99]. We reserve several of these questions for future work.

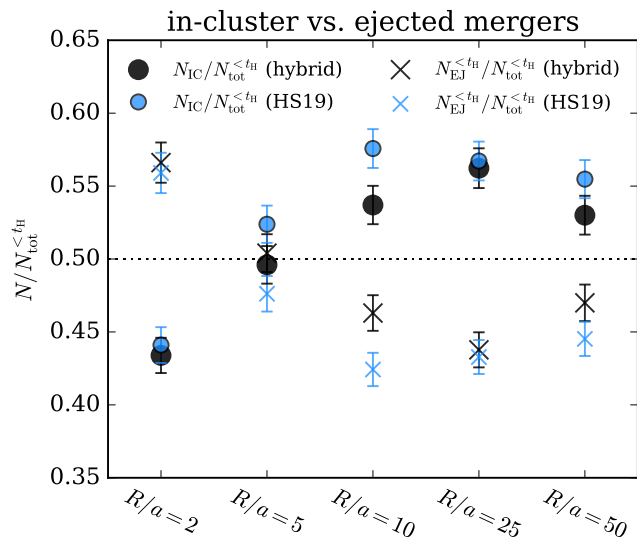


FIG. 12. Number of in-cluster BBH mergers (*circle*), N_{IC} , and ejected BBHs with $\tau < t_H$ (*cross*), $N_{EJ}^{<t_H}$, each scaled by the total number of mergers, $N_{tot}^{<t_H} = N_{IC} + N_{EJ}^{<t_H}$. Results are derived using our numerical scheme outlined in Section III A 3 and our ‘fiducial cluster parameters’ together with our ‘hybrid approach’ described in Section III B, for different values of R_p/a (x-axis). The *black symbols* show results from our hybrid approach, where the *blue symbols* show results from our analytical MC approach. As seen, if only strong encounters are included ($R_p/a = 2$) the fractions $N_{IC}/N_{tot}^{<t_H}$ and $N_{EJ}^{<t_H}/N_{tot}^{<t_H}$ are about 0.45 and 0.55, respectively, i.e. ejected BBH mergers dominate the merging population. However, when we increase R_p/a , and thereby start to include weak encounters, more and more of the BBHs tend to merge inside the cluster before ejection becomes possible. Despite some Poisson scatter, this statement is consistent for both the hybrid and the analytical approach. That the inclusion of weak interactions seems to increase the relative number of in-cluster mergers has major implications for, e.g., predicting accurate GW peak frequency and eccentricity distributions observable by especially LISA. It can also impact the number of 2. generation GW mergers.

C. Fast Analytical Monte Carlo Approach

We finish this section by exploring how well one can do by using Eq. (6) for all weak interactions, i.e. for all $r_p/a_0 > \mathcal{C}(=2)$, instead of employing our hybrid approach that includes numerical simulations; an approach we refer to as our ‘Analytical MC Approach’. In this approach it is unavoidable to encounter situations where either $e > 1$ or $e < 0$, also when using the SO term, therefore, every time such a case appears we simply put $\Delta e = 0$ without stopping the code. Results from this approach is shown in Fig. 10 and 12. As seen, despite some Poisson scatter, the Analytical MC Approach seems to perform very well. A great overlap between the hybrid and the analytical MC approach is especially seen in Fig. 10, where both of them clearly distinguish them-

selves from the runs where only strong interactions are included.

This is highly encouraging as the analytical MC approach is extremely fast and easy to code up, which especially allows one to explore a wide range of cluster parameters in a very short amount of time. This approach is therefore also well suited for performing a more systematic study on the importance of weak interactions as function of the properties of the cluster and the interacting BHs.

Finally, there are several easy ways of improving our proposed analytical MC approach, two of which are: (1) For strong interactions use the full distribution of δ given e.g. in [78], instead of the average value $\delta = 7/9$. (2) For weak interactions, include the change in SMA Δa using [100], instead of simply assuming $\Delta a = 0$. On top of these, it is possible to improve on the distribution of 3-body mergers, and also include 4-body mergers. In an upcoming paper we will quantify the role of single-single GW capture mergers. All of these studies will become central in developing the next generation of fast MC codes for modeling dense stellar systems and their formation of BBH GW mergers.

IV. CONCLUSIONS

We have in this paper quantified the effects from weak encounters on the assembly of BBH mergers in GCs using a combination of novel analytical and numerical techniques. Current state-of-the-art codes [e.g. 67, 83], as well as recent analytical studies [e.g. 55, 56] have only included strong interactions in their modeling; however, BBHs in GCs will in-between each strong interaction undergo hundreds of weak interactions, each of which changes the eccentricity of the BBH slightly and thereby its GW inspiral life time. It is therefore possible for BBHs to both be driven towards merger and also away from merger entirely through weak interactions.

Using a simple cluster model with the inclusion of weak and strong interactions, we find here that the addition of weak interactions leads to a notable and systematic relative increase in the number of BBHs merging in-side the cluster. For our fiducial cluster parameters we find that the total number of observable BBH mergers goes from being dominated by ejected mergers to in-cluster mergers when weak interactions are included. Because of the relative short GW inspiral time of in-cluster mergers, this population will appear as eccentric LISA sources, and therefore add an important piece to the puzzle of how to disentangle BBH merger channels from each other by the use of GW observations.

Our main results are based on a hybrid approach where we combine full 2.5PN numerical scattering experiments with analytical expressions. We have in this regard especially demonstrated that very similar results are achieved if one uses our new SO perturbative solution [86] for modeling the changes in BBH eccentricity for all weak inter-

actions. This is highly encouraging, as this allows for a full analytical MC modeling of the problem including both weak and strong interactions as well as 2.5PN effects. This makes it e.g. possible to derive distributions of BBH merger properties in just a few seconds for any cluster parameters. Of course, this approach is based on a simplified cluster model, but previous work based on the same assumptions turns out to be in surprisingly good agreement with more sophisticated MC models [e.g. 47].

We have in this paper only considered results from a single set of cluster parameters, but we plan in the near future to explore the relative importance of weak interactions for a range of cluster parameters from less dense to very dense nuclear star clusters. It might be that in some regimes weak interactions play an even larger role than found in this paper; however, we reserve that for future work.

Finally, we note that the weak interactions we have here considered are essential to include for studying the secular evolution of BBHs in e.g. non-spherical clusters [97, 98]. The reason is that weak interactions not only give rise to a change in eccentricity, but also to a change in the orbital orientation. This change can interfere with the secular change induced from a non-spherical potential, and thereby affect the distribution of BBHs driven to merger in-side clusters through this mechanism. Whether or not this is a competing channel for forming eccentric LISA sources will be studied in upcoming work.

Acknowledgments. — We thank Stephen McMillan and Piet Hut for stimulating discussions. J.S. acknowledges support from the Lyman Spitzer Fellowship. A.S.H. gratefully acknowledges support from the Institute for Advanced Study, and the Martin A. and Helen Chooljian Membership.

-
- [1] B. P. Abbott *et al.*, Physical Review Letters **116**, 061102 (2016), 1602.03837.
- [2] B. P. Abbott *et al.*, Physical Review Letters **116**, 241103 (2016), 1606.04855.
- [3] B. P. Abbott *et al.*, Physical Review X **6**, 041015 (2016), 1606.04856.
- [4] B. P. Abbott *et al.*, Physical Review Letters **118**, 221101 (2017), 1706.01812.
- [5] B. P. Abbott *et al.*, Physical Review Letters **119**, 141101 (2017), 1709.09660.
- [6] B. Zackay, T. Venumadhav, L. Dai, J. Roulet, and M. Zaldarriaga, arXiv e-prints, arXiv:1902.10331 (2019), 1902.10331.
- [7] T. Venumadhav, B. Zackay, J. Roulet, L. Dai, and M. Zaldarriaga, arXiv e-prints, arXiv:1904.07214 (2019), 1904.07214.
- [8]
- [9] B. P. Abbott *et al.*, Physical Review Letters **119**, 161101 (2017), 1710.05832.
- [10] M. Dominik *et al.*, Astrophys. J. **759**, 52 (2012), 1202.4901.
- [11] M. Dominik *et al.*, Astrophys. J. **779**, 72 (2013), 1308.1546.
- [12] M. Dominik *et al.*, Astrophys. J. **806**, 263 (2015), 1405.7016.
- [13] K. Belczynski *et al.*, Astrophys. J. **819**, 108 (2016), 1510.04615.
- [14] K. Belczynski, D. E. Holz, T. Bulik, and R. O’Shaughnessy, Nature (London) **534**, 512 (2016), 1602.04531.
- [15] K. Silsbee and S. Tremaine, Astrophys. J. **836**, 39 (2017), 1608.07642.
- [16] A. Murguia-Berthier, M. MacLeod, E. Ramirez-Ruiz, A. Antoni, and P. Macias, Astrophys. J. **845**, 173 (2017), 1705.04698.
- [17] C. L. Rodriguez and F. Antonini, Astrophys. J. **863**, 7 (2018), 1805.08212.
- [18] S. L. Schröder, A. Batta, and E. Ramirez-Ruiz, Astrophys. J. Lett. **862**, L3 (2018), 1805.01269.
- [19] S. F. Portegies Zwart and S. L. W. McMillan, Astrophys. J. **528**, L17 (2000).
- [20] S. Banerjee, H. Baumgardt, and P. Kroupa, Mon. Not. Roy. Astron. Soc. **402**, 371 (2010), 0910.3954.
- [21] A. Tanikawa, Mon. Not. Roy. Astron. Soc. **435**, 1358 (2013), 1307.6268.
- [22] Y.-B. Bae, C. Kim, and H. M. Lee, Mon. Not. Roy. Astron. Soc. **440**, 2714 (2014), 1308.1641.
- [23] C. L. Rodriguez *et al.*, Physical Review Letters **115**, 051101 (2015), 1505.00792.
- [24] C. L. Rodriguez, S. Chatterjee, and F. A. Rasio, Phys. Rev. D **93**, 084029 (2016), 1602.02444.
- [25] C. L. Rodriguez, C.-J. Haster, S. Chatterjee, V. Kalogera, and F. A. Rasio, Astrophys. J. Lett. **824**, L8 (2016), 1604.04254.
- [26] A. Askar, M. Szkudlarek, D. Gondek-Rosińska, M. Giersz, and T. Bulik, Mon. Not. Roy. Astron. Soc. **464**, L36 (2017), 1608.02520.
- [27] D. Park, C. Kim, H. M. Lee, Y.-B. Bae, and K. Belczynski, Mon. Not. Roy. Astron. Soc. **469**, 4665 (2017), 1703.01568.
- [28] I. Bartos, B. Kocsis, Z. Haiman, and S. Márka, Astrophys. J. **835**, 165 (2017), 1602.03831.
- [29] N. C. Stone, B. D. Metzger, and Z. Haiman, Mon. Not. Roy. Astron. Soc. **464**, 946 (2017), 1602.04226.
- [30] B. McKernan *et al.*, ArXiv e-prints (2017), 1702.07818.
- [31] R. M. O’Leary, B. Kocsis, and A. Loeb, Mon. Not. Roy. Astron. Soc. **395**, 2127 (2009), 0807.2638.
- [32] J. Hong and H. M. Lee, Mon. Not. Roy. Astron. Soc. **448**, 754 (2015), 1501.02717.
- [33] J. H. VanLandingham, M. C. Miller, D. P. Hamilton, and D. C. Richardson, Astrophys. J. **828**, 77 (2016), 1604.04948.
- [34] F. Antonini and F. A. Rasio, Astrophys. J. **831**, 187 (2016), 1606.04889.
- [35] A. P. Stephan *et al.*, Mon. Not. Roy. Astron. Soc. **460**, 3494 (2016), 1603.02709.
- [36] B.-M. Hoang, S. Naoz, B. Kocsis, F. A. Rasio, and F. Dosopoulou, ArXiv e-prints (2017), 1706.09896.
- [37] A. S. Hamers, B. Bar-Or, C. Petrovich, and F. Antonini, Astrophys. J. **865**, 2 (2018), 1805.10313.

- [38] A. Loeb, *Astrophys. J. Lett.* **819**, L21 (2016), 1602.04735.
- [39] S. E. Woosley, *Astrophys. J. Lett.* **824**, L10 (2016), 1603.00511.
- [40] A. Janiuk, M. Bejger, S. Charzyński, and P. Sukova, *ArXiv e-prints* **51**, 7 (2017), 1604.07132.
- [41] D. J. D’Orazio and A. Loeb, *ArXiv e-prints* (2017), 1706.04211.
- [42] S. Bird *et al.*, *Physical Review Letters* **116**, 201301 (2016), 1603.00464.
- [43] I. Cholis *et al.*, *Phys. Rev. D***94**, 084013 (2016), 1606.07437.
- [44] M. Sasaki, T. Suyama, T. Tanaka, and S. Yokoyama, *Physical Review Letters* **117**, 061101 (2016), 1603.08338.
- [45] B. Carr, F. Kühnel, and M. Sandstad, *Phys. Rev. D***94**, 083504 (2016), 1607.06077.
- [46] J. Lopez, Martin, A. Batta, E. Ramirez-Ruiz, I. Martinez, and J. Samsing, *Astrophys. J.***877**, 56 (2019), 1812.01118.
- [47] J. Samsing *et al.*, *arXiv e-prints*, *arXiv:1901.02889* (2019), 1901.02889.
- [48] K. Kremer, W. Lu, C. L. Rodriguez, M. Lachat, and F. Rasio, *arXiv e-prints*, *arXiv:1904.06353* (2019), 1904.06353.
- [49] N. Seto and K. Kyutoku, *Physical Review Letters* **118**, 151101 (2017), 1611.05875.
- [50] G. Fragione, N. Leigh, R. Perna, and B. Kocsis, *arXiv e-prints*, *arXiv:1905.09471* (2019), 1905.09471.
- [51] Y. Meiron, B. Kocsis, and A. Loeb, *Astrophys. J.***834**, 200 (2017), 1604.02148.
- [52] L. Randall and Z.-Z. Xianyu, *arXiv e-prints*, *arXiv:1805.05335* (2018), 1805.05335.
- [53] C. L. Rodriguez, M. Zevin, C. Pankow, V. Kalogera, and F. A. Rasio, *Astrophys. J. Lett.* **832**, L2 (2016), 1609.05916.
- [54] W. M. Farr *et al.*, *ArXiv e-prints* (2017), 1706.01385.
- [55] J. Samsing and D. J. D’Orazio, *Mon. Not. Roy. Astron. Soc.* (2018), 1804.06519.
- [56] D. J. D’Orazio and J. Samsing, *Mon. Not. Roy. Astron. Soc.* **481**, 4775 (2018), 1805.06194.
- [57] K. Kremer *et al.*, *Phys. Rev. D***99**, 063003 (2019), 1811.11812.
- [58] K. Gültekin, M. C. Miller, and D. P. Hamilton, *Astrophys. J.***640**, 156 (2006).
- [59] J. Samsing, M. MacLeod, and E. Ramirez-Ruiz, *Astrophys. J.***784**, 71 (2014), 1308.2964.
- [60] J. Samsing and E. Ramirez-Ruiz, *Astrophys. J. Lett.* **840**, L14 (2017), 1703.09703.
- [61] J. Samsing and T. Ilan, *Mon. Not. Roy. Astron. Soc.* **476**, 1548 (2018), 1706.04672.
- [62] J. Samsing, M. MacLeod, and E. Ramirez-Ruiz, *Astrophys. J.***853**, 140 (2018), 1706.03776.
- [63] J. Samsing and T. Ilan, *Mon. Not. Roy. Astron. Soc.* **482**, 30 (2019), 1709.01660.
- [64] J. Samsing, *Phys. Rev. D***97**, 103014 (2018), 1711.07452.
- [65] J. Samsing, A. Askar, and M. Giersz, *Astrophys. J.***855**, 124 (2018), 1712.06186.
- [66] M. Zevin, J. Samsing, C. Rodriguez, C.-J. Haster, and E. Ramirez-Ruiz, *Astrophys. J.***871**, 91 (2019), 1810.00901.
- [67] C. L. Rodriguez *et al.*, *Phys. Rev. D***98**, 123005 (2018), 1811.04926.
- [68] T. A. Thompson, *Astrophys. J.***741**, 82 (2011).
- [69] L. Randall and Z.-Z. Xianyu, *Astrophys. J.***864**, 134 (2018), 1802.05718.
- [70] G. Fragione, E. Grishin, N. W. C. Leigh, H. B. Perets, and R. Perna, *arXiv e-prints*, *arXiv:1811.10627* (2018), 1811.10627.
- [71] L. Randall and Z.-Z. Xianyu, *arXiv e-prints*, *arXiv:1902.08604* (2019), 1902.08604.
- [72] G. Fragione, N. Leigh, and R. Perna, *arXiv e-prints*, *arXiv:1903.09160* (2019), 1903.09160.
- [73] G. Fragione and A. Loeb, *Mon. Not. Roy. Astron. Soc.* **486**, 4443 (2019), 1903.10511.
- [74] G. Fragione and O. Bromberg, *arXiv e-prints*, *arXiv:1903.09659* (2019), 1903.09659.
- [75] G. Fragione and B. Kocsis, *Mon. Not. Roy. Astron. Soc.* **486**, 4781 (2019), 1903.03112.
- [76] B. Kocsis and J. Levin, *Phys. Rev. D* **85**, 123005 (2012).
- [77] L. Gondán, B. Kocsis, P. Raffai, and Z. Frei, *Astrophys. J.***860**, 5 (2018), 1711.09989.
- [78] D. C. Heggie, *Mon. Not. Roy. Astron. Soc.* **173**, 729 (1975).
- [79] S. J. Aarseth and D. C. Heggie, *Astron. and Astrophys.* **53**, 259 (1976).
- [80] P. Hut and J. N. Bahcall, *Astrophys. J.***268**, 319 (1983).
- [81] A. Askar, M. Arca Sedda, and M. Giersz, *Mon. Not. Roy. Astron. Soc.* **478**, 1844 (2018), 1802.05284.
- [82] M. Arca Sedda, A. Askar, and M. Giersz, *Mon. Not. Roy. Astron. Soc.* **479**, 4652 (2018), 1801.00795.
- [83] M. Giersz, D. C. Heggie, J. R. Hurley, and A. Hypki, *Mon. Not. Roy. Astron. Soc.* **431**, 2184 (2013), 1112.6246.
- [84] L. Blanchet, *Living Reviews in Relativity* **17** (2014), 1310.1528.
- [85] J. Samsing, M. MacLeod, and E. Ramirez-Ruiz, *Astrophys. J.***846**, 36 (2017), 1609.09114.
- [86] A. S. Hamers and J. Samsing, *arXiv e-prints*, *arXiv:1904.09624* (2019), 1904.09624.
- [87] D. C. Heggie and F. A. Rasio, *Mon. Not. Roy. Astron. Soc.* **282**, 1064 (1996), astro-ph/9506082.
- [88] S. Naoz, *Annual Rev. of Astron. and Astrophys.* **54**, 441 (2016), 1601.07175.
- [89] A. M. Geller, N. W. C. Leigh, M. Giersz, K. Kremer, and F. A. Rasio, *Astrophys. J.***872**, 165 (2019), 1902.00019.
- [90] P. Peters, *Phys. Rev.* **136**, B1224 (1964).
- [91] J. Samsing, N. W. C. Leigh, and A. A. Trani, *Mon. Not. Roy. Astron. Soc.* **481**, 5436 (2018), 1803.08215.
- [92] G. Li, S. Naoz, B. Kocsis, and A. Loeb, *Astrophys. J.***785**, 116 (2014), 1310.6044.
- [93] V. V. Sidorenko, *Celestial Mechanics and Dynamical Astronomy* **130**, 4 (2018), 1708.06001.
- [94] S. Naoz, B. Kocsis, A. Loeb, and N. Yunes, *Astrophys. J.***773**, 187 (2013), 1206.4316.
- [95] S. Weinberg, *Gravitation and Cosmology: Principles and Applications of the General Theory of Relativity* (, 1972).
- [96] J. Samsing and D. J. D’Orazio, *Phys. Rev. D***99**, 063006 (2019), 1807.08864.
- [97] C. Hamilton and R. R. Rafikov, *arXiv e-prints*, *arXiv:1902.01344* (2019), 1902.01344.
- [98] C. Hamilton and R. R. Rafikov, *arXiv e-prints*, *arXiv:1902.01345* (2019), 1902.01345.
- [99] R. M. O’Leary, Y. Meiron, and B. Kocsis, *Astrophys. J. Lett.* **824**, L12 (2016), 1602.02809.
- [100] A. Roy and M. Haddow, *Celestial Mechanics and Dynamical Astronomy* **87**, 411 (2003).